SCIENCE CHINA PRESS

SCIENCE CHINA Chemistry
https://doi.org/10.1007/s11426-025-3309-6

REVIEWS

Ionic liquids in aqueous zinc metal batteries using mild electrolytes: from electrolyte engineering to interfacial chemistry

Huifang Fei[1], Fuhua Yang[3,4*] & Junnan Hao[2*]

[1]College of Materials Science and Engineering, Nanjing Tech University, Nanjing 211816, China
[2]School of Chemical Engineering, The University of Adelaide, Adelaide 5005, Australia
[3]Helmholtz Institute Ulm (HIU), Ulm 89081, Germany
[4]Karlsruhe Institute of Technology (KIT), Karlsruhe 76021, Germany

Published in virtual special issue "Advanced Aqueous Batteries"
*Corresponding authors (email: fuhua.yang@csu.edu.cn; junnan.hao@adelaide.edu.au)

Received 30 November 2025; Accepted 21 January 2026; Published online 9 June 2026

Abstract Aqueous zinc metal batteries (AZMBs) are considered as promising candidates for grid-scale energy storage systems because of the abundance of zinc reserves, high theoretical capacity of zinc anode, and intrinsic safety of the aqueous electrolytes. However, zinc anodes in aqueous electrolytes suffer from severe issues, such as H_2 evolution, dendrite growth, and spontaneous corrosion, resulting in poor reversibility and lifespan. Introducing ionic liquids (ILs) with tunable structures and superior physicochemical properties offers a viable solution. This strategy modulates both the bulk electrolyte and the interfacial environment, thereby addressing these challenges. This review outlines the recent progress in ILs for AZMBs employing mild electrolytes, emphasizing electrolyte design strategies and interfacial chemistry. We begin by introducing the fundamental properties of ILs relevant to AZMBs. Subsequently, we elucidate their specific roles and functions within the electrolyte, followed by an analysis of the modified interfacial chemistry at the anode. Finally, the remaining challenges associated with IL utilization are examined, and a potential future direction for the practical development of IL-based electrolytes in AZMBs is proposed.

Keywords zinc metal batteries, ionic liquid, mild aqueous electrolytes, electrolyte engineering, interfacial chemistry

1 Introduction

The first rechargeable Zn-based aqueous battery employing mild electrolyte (2 M $ZnSO_4$) was created in 1986 by Yamamoto and Shoji [1]. Afterwards, aqueous zinc metal batteries (AZMBs) in mild aqueous electrolytes regained tremendous attention during the past decade because of their great potential in the application of grid-scale energy storage systems which requires high-level safety and low cost as well [2]. Among various aqueous batteries with different charge carriers (monovalent Li^+, Na^+, K^+, NH_4^+ and multivalent Ca^{2+}, Mg^{2+}, Al^{3+}) [3–5], AZMBs stand out since Zn metal anode possesses the proper redox potential (−0.76 V *vs.* standard hydrogen electrode) of Zn/Zn^{2+}, high abundance, well-established manufacturing and recycling technologies, and high energy density (820 mAh g^{-1} for gravimetric and 5855 mAh cm^{-3} for volumetric) [6–8]. Meanwhile, the advantages of aqueous electrolytes include fast ionic transport and environmental benignity as well [9,10]. However, the utilization of aqueous mild electrolytes (defined herein as having an operational pH range of 3.0–8.0) [11,12] and Zn metal anode together bring a lot of challenges, such as poor Coulombic efficiency (CE) and short lifespan of Zn anodes caused by dendrite formation and side reactions (hydrogen evolution and corrosion) [2,13,14]. Specifically, pure water exhibits narrow theoretical electrochemical stability window (ESW) of 1.23 V and diluted aqueous electrolytes merely have increased ESW of ~1.9 V [9,15]. Supposing that the pH value of the designed electrolyte is 7, the theoretical onset potential of hydrogen evolution reaction (HER) is −0.413 V *vs.* standard hydrogen electrode ($E_{H_2} = -0.059 \times pH$), which is higher than the redox potential of Zn/Zn^{2+} [2]. Even though Zn metal anode exhibits certain overpotential towards HER, HER inevitably happens during the stripping/plating processes of Zn, which heavily impact the CE and stability of the battery [8,16]. The horrible HER is detrimental as it is responsible for elevating the local pH at the Zn surface, which promotes the formation of the passivating by-product $Zn_4(OH)_6SO_4{\cdot}xH_2O$ [2]. Meanwhile, Zn spontaneously corrodes in aqueous electrolyte, generating identical passivation layer. The poorly electronic and ionic-conductive passivation parts will cause uneven distribution of electric field in Zn, therefore resulting in uncontrolled growth of Zn dendrites [17]. Besides, the rampant dendrite growth will finally penetrate the separator and leads to short circuit.

Based on the above background, several categories of effective strategies have been developed to solve the challenges, including Zn electrode construction [18,19], separator modification [20], and electrolyte engineering [21–23]. Among these, electrolyte engineering is particularly pivotal, as it targets the root cause of undesirable reactions at the electrode/electrolyte interface, like HER, corrosion, and dendrite formation [24–26]. Therefore, electrolytes not only connect cathodes and anodes by ion diffusion but also directly determine the electrochemical performance of Zn metal anodes. Ionic liquids (ILs), composed of cations and anions, possess tunable physicochemical properties, rendering them attractive as co-salts or additives for designing functional electrolytes aimed at enhancing the electrochemical performance of Zn anodes [27,28]. Generally

Citation: Fei H, Yang F, Hao J. Ionic liquids in aqueous zinc metal batteries using mild electrolytes: from electrolyte engineering to interfacial chemistry. *Sci China Chem*, https://doi.org/10.1007/s11426-025-3309-6

speaking, IL has advantages with wide ESW, excellent thermal/chemical stability, an acceptable level of ionic conductivity and intrinsic inflammability, which have been widely utilized in nonaqueous alkaline-metal batteries [29]. During the past decade, IL-based aqueous electrolytes have been intensively investigated in AZMBs with the objective of boosting the electrochemical performance of Zn metal anodes [27]. The protection mechanism of these approaches for stable Zn anodes mainly includes (Figure 1): (1) breaking the H-bonds of water and reorganizing the inner solvation structure of Zn; (2) constructing the *in-situ* formation of solid electrolyte interphase (SEI); (3) suppressing the tip effect to induce uniform Zn deposition.

The application of IL-based aqueous electrolytes in AZMBs has proliferated significantly, particularly over the past five years. Despite this growing interest, few reviews have systematically clarified the interactions between different species of IL-based electrolytes and their modifying effects on the interfacial chemistry at the electrode/electrolyte interface. Given the structural diversity of ILs, different ions can profoundly influence the physicochemical and electrochemical properties of aqueous electrolytes, accordingly, impacting the performance of Zn anodes. Understanding the mechanisms behind the improved electrochemical performance of zinc anodes can guide the purposeful molecular design of ILs. In this review, we provide a comprehensive overview of the roles of ILs in AZMBs. We begin with an introduction to the fundamental properties of ILs, followed by a discussion of their behavior and functions in aqueous electrolytes. Afterwards, we focus on IL-mediated interfacial chemistry, including modifications to EDL and the formation of SEI. Finally, the challenges of IL utilization are discussed, followed by a proposed future direction for the practical development of IL-based electrolytes in AZMBs. We hope this review will stimulate further interest in IL-based electrolytes, thereby paving the way for the application of AZMBs in grid-scale energy storage.

2 Fundamentals of ILs relevant to AZMBs

2.1 Classification of ILs

ILs are normally described as compounds completely consisting of ions with a melting point of below 100 °C [34]. The invention of the first room-temperature IL, ethyl ammonium nitrate, could be traced back to 1914, reported by Walden's group [35]. Then in 1992, Wilkes's group [36] synthesized 1-ethyl-3-methylimidazolium tetrafluoroborate ([EMIM]BF_4), an air/water-stable IL with strong chemical stability, making the wide use of IL possible [37]. Since then, task-specific ILs were introduced, *i.e.*, by tuning the functional groups of cations and anions to achieve specific chemistry or bioactivity [38]. Specifically, the combination of different cations and anions heavily impacts the physicochemical properties of ILs, such as viscosity, melting point, ionic conductivity, chemical/electrochemical stability, hydrophilicity, hydrophobicity, and so on [39]. The physical properties, including viscosity and ionic conductivity of several commonly used ILs in AZMBs, were summarized in Table 1.

The typical structures of ILs are demonstrated in Figure 2, including cations and anions. These ILs are commonly categorized into two important groups according to the types of contained cation: protic and aprotic [40]. Protic ILs refer to those whose cations are generated by a proton transfer reaction between the interactions of Brønsted acid and base, keeping labile protons (*i.e.*, N–H) [41]. For example, triethylammonium and 1-methylimidazolium-based ILs are protic ILs. Those ILs normally come from exchange reactions between organic compounds with alkyl halides,

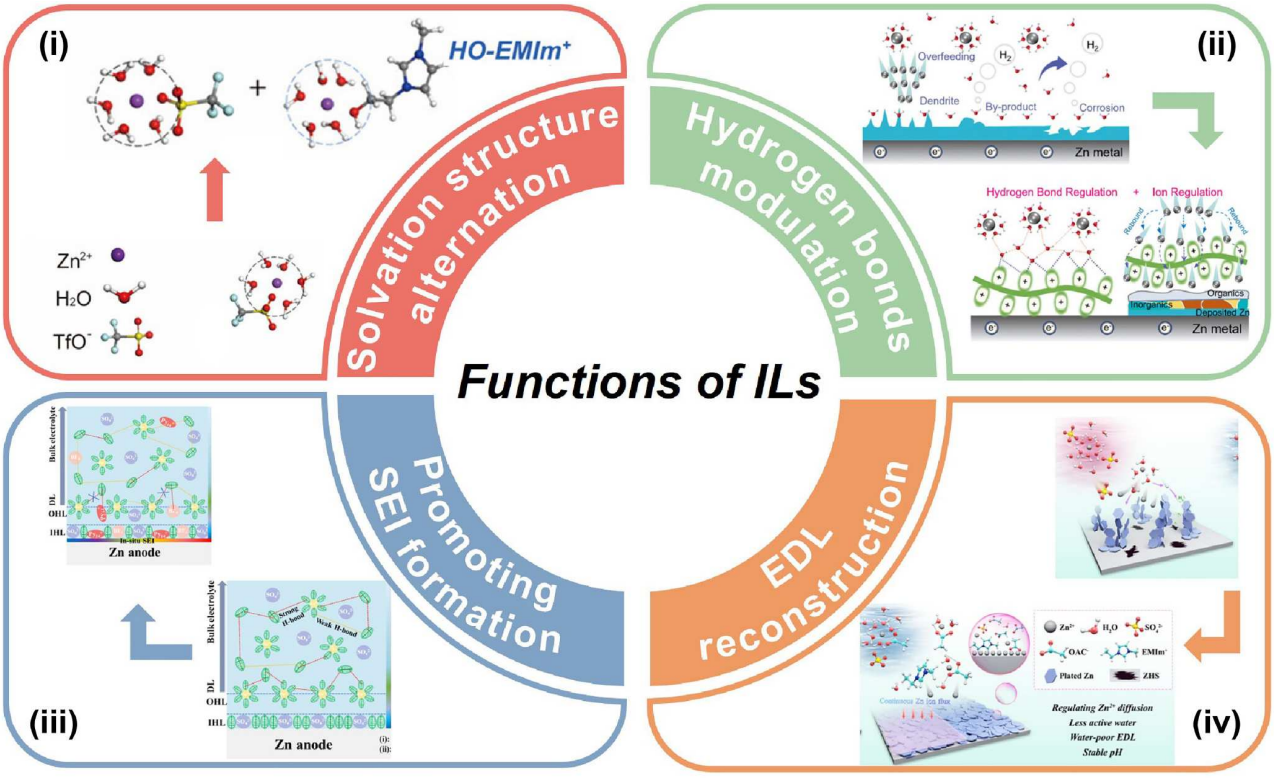

Figure 1 (Color online) Summary of protection mechanisms of IL for stable zinc anodes. (i) Solvation structure alternation. Reproduced with permission from Ref. [30]. Copyright©2025, Wiley-VCH. (ii) Hydrogen bond modulation. Reproduced with permission from Ref. [31]. Copyright©2025, the Royal Society of Chemistry. (iii) Promoting SEI formation. Reproduced with permission from Ref. [32]. Copyright©2025, Elsevier. (iv) Electric double layer (EDL) reconstruction. Reproduced with permission from Ref. [33]. Copyright©2025, Elsevier.

Table 1 Physical properties, including viscosity, ionic conductivity, and melting point of several commonly used ILs for stabilizing Zn anode in AZMBs

ILs	Viscosity (mPa s)	Ionic conductivity (mS cm^{-1})	Melting point (°C)	Ref.
[BMIM]OTF[a)]	90	3.7	16	[36]
[EMIM]OTF	42.9	9.29	−9	[37,38]
[BMIM]TFSI[b)]	52	3.9	−4	[36]
[EMIM]OAc[c)]	143.6	2.96	–	[39]
[EMIM]FSI[d)]	19	17.74	–	[29]
[EMIM]BF_4	37.7	14	12.5	[37]
[BMIM]PF_6[e)]	1.4	312	−8	[36]

a) $[BMIM]^+$ is the abbreviation of 1-butyl-2,3-dimethylimidazolium cation; OTF^- is the abbreviation of triflate anion. b) $TFSI^-$ is the abbreviation of bis-(trifluoromethanesulfonyl)imide anion. c) OAc^- is the abbreviation of acetate anion. d) FSI^- is the abbreviation of bis(fluorosulfonyl)imide anion. e) PF_6^- is the hexafluorophosphate anion.

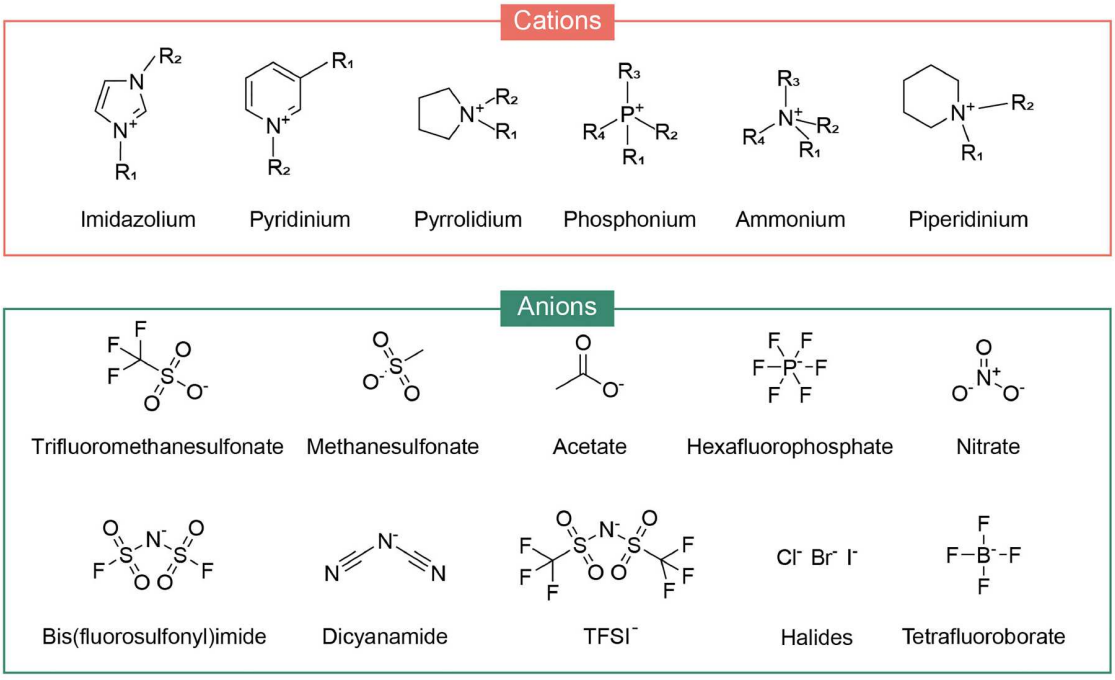

Figure 2 (Color online) Chemical structures of typical cations and anions in ILs.

without interchangeable protons, are defined as aprotic ILs [42], such as ILs containing $[BMIM]^+$ and $[EMIM]^+$. Finally, there is a special kind of IL analogue, deep eutectic solvents (DESs), which are not considered identical as the traditional ILs but have similar physical properties as ILs, such as low vapor pressure, high ionic conductivity and low melting point. DESs, eutectic mixtures, are normally composed of H-bond donors and H-bond acceptors, formed by H-bonds.

2.2 Viscosity

Most ILs are viscous at room temperature, with viscosities comparable to those of oils, typically two to three times higher than the viscosity of conventional organic solvents [34]. Their viscosity values broadly range from 0.7 to as high as 257000 mPa s [43]. Generally speaking, the viscosity of ILs mainly arises from the interactions between cations and anions [44]. Furthermore, increasing the length of the alkyl chains on the cations does not invariably lead to higher viscosity, while the types of anions significantly influence the viscosity of ILs [45]. It is currently well-established that insufficient data exists to draw a definitive conclusion. The high viscosity leads to inferior rate capability, lower reaction kinetics, *etc*., which violates part intrinsic advantages of aqueous electrolytes. Thus, the amount of ILs utilized in aqueous electrolytes should be carefully evaluated in order to reach a balance between electro/chemical stability, ionic conductivity and viscosity.

2.3 Hydrophilicity/hydrophobicity

The hydrophilicity/hydrophobicity of ILs is mainly determined by the properties of anions. Hydrophilic anions normally include Cl^-, BF_4^-, CH_3COO^-, and NO_3^- while PF_6^-, $TFSI^-$, and FSI^- are hydrophobic [40]. For example, [EMIM]Cl is hydrophilic, but [EMIM]TFSI is hydrophobic. If the anion is fixed, the longer the alkyl chain, the lower the solubility of the IL in water [41]. The interactions of ILs in aqueous electrolytes are quite complicated. After dissolving, the hydrophilic anions are able to interrupt the H-bonds between water molecules in diluted aqueous electrolytes. For protic ILs, the N–H groups on cations can form H-bonds with water as well, further reducing water activity. Even though some ILs are insoluble in pure water, they can be dissolved with the help of solutes. For example, [EMIM]FSI, intrinsically hydrophobic, is soluble in 3 M $Zn(OTF)_2$ aqueous solution [42].

2.4 Melting point

The typical definition of ILs ensures that the melting point is below

100 °C. The factors affecting the melting point of a substance are van der Walls interactions, charge distribution, H-bonds formation and the symmetry of ions [44]. By comparing the melting point of organic salt (*e.g.*, the melting point of NaCl is 803 °C) and traditional IL (*e.g.*, the melting point of is 84 °C), it can be seen that the reduction of melting point in IL is attributed to the replacement of small inorganic cation by big-size asymmetrical organic cations [34]. In aqueous electrolytes, dissolved ILs profoundly impact the thermal behavior, *i.e.*, decreasing the melting point and enhancing the anti-freezing resistance, via extensive interactions with water molecules.

2.5 Ionic conductivity

In battery applications, the ionic conductivity of ILs generally falls within the range of 0.1 to 18 mS cm^{-1}, with the actual value determined by the number of available charge carriers and their mobility [46]. The stronger interactions between different species in ILs will result in lower mobility. Therefore, the ionic conductivity is higher when there are fewer ion interactions and more delocalized charges. For example, strong Brønsted acids and bases have higher ionic conductivity. Moreover, the ionic conductivity is lower if the size of cations in ILs is larger (lower mobility), as exemplified by the lower ionic conductivity of 1-benzyl-2-ethylimidazolium-based ILs in comparison with 1-methyl-2-methylimidazolium-based ILs [47].

2.6 Electro/chemical stability

Multiple elements impact the electrochemical stability of ILs, highly associated with the specific structures of the composed cations and anions. Among anions, the anti-oxidized ability varies from type to type. For example, BF_4^- and PF_6^- are more stable than the organic counterparts such as $TFSI^-$ and OTF^- at higher potentials [48]. In terms of the cations, the structures are highly variable, including different cation types, functional groups on the side chain, alkyl chain length and position of the substituents [44]. Normally, imidazolium, pyridinium and ammonium demonstrate weaker electrochemical stability than pyrrolidinium, piperidinium and phosphonium cations. Besides, reduced chain length and functionalization cannot assure the increase of electrochemical stability, which is simultaneously affected by the nature of the cations and anions and the interactions between them.

3 Design strategies for IL-based electrolytes in AZMBs

In traditional aqueous electrolytes of zinc batteries, commonly used salts include $ZnSO_4$, $Zn(CH_3COO)_2$, $Zn(OTF)_2$, $Zn(ClO_4)_2$, and $Zn(NO_3)_2$. Water, characterized by its high dielectric constant and polarity, tends to coordinate zinc ions *via* the long pair electrons of oxygen atoms in water molecules [9]. This coordination is dominant in mild dilute electrolytes, where water is abundant, leading to the formation of a primary $[Zn(H_2O)_6]^{2+}$ solvation shell with negligible anion involvement (Figure 3). The deprotonation energy of solvated water molecules is confirmed to be lower than that of non-solvated water due to the strong interactions between O atom in water and Zn^{2+}, thus leading to reduced O–H bond strength [49]. This means deprotonation in solvated water is energetically favorable, underscoring higher risk of HER. Consequently, HER results in local pH increase and the formation of corrosion by-product which further covers the active sites and hinders the kinetics of Zn stripping/plating. Therefore, altering the primary solvation structure of Zn^{2+} is an effective strategy to boost the electrochemical performance of Zn anodes, which not only reduces the amount of solvated water, but also elevates the deprotonation energy of solvated water molecules which makes them harder to decompose [50]. Apart from the solvated water, the activity of non-solvated water molecules in the electrolytes is also critical to the electrochemical performance of Zn anodes [24]. These non-solvated water molecules can exist in different states, which are determined by their local hydrogen-bonding environments, including free O–H vibration, DA (single donor-single acceptor), DDA (double donor-single acceptor), DAA (single donor-double acceptor), or DDAA (double donor-double acceptor) [51]. According to Grotthuss mechanism, the continuous H-bonds network between water molecules facilitates fast proton migration which enhance HER risk [52]. Additionally, non-solvated water molecules tend to adsorb onto the Zn surface, thereby increasing the interfacial water content and consequently aggravating side reactions. Thus, the modulation of hydrogen bonding and the solvation structure are both critical considerations in electrolyte design.

The design of IL-based electrolytes for AZMBs has emerged as an effective strategy to tackle the above-mentioned challenges. Thanks to the advantages of interactions between cations and anions, strong electrochemical stability, tunable structures and nonvolatility of IL, the enrollment of ILs in aqueous electrolytes provides flexible ways to overcome the shortcomings [27]. How ILs integrate with traditional aqueous electrolytes dictates the role they play and the form they adopt. In this regard, we review the design strategies for IL-based electrolytes, categorized by the method of IL introduction into the electrolyte with a focus on the interactions among various species within the electrolytes.

3.1 Pure IL-based electrolytes

Even though the viscosity and cost of pure conventional ILs as electrolytes remain high, they can provide a water-free environ-

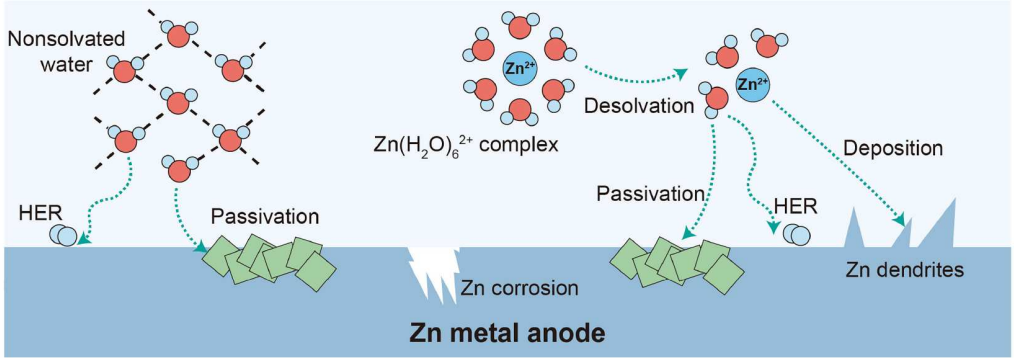

Figure 3 (Color online) Schematic illustration of side reactions on Zn anodes induced by the bulk-electrolyte structure in diluted mild aqueous electrolytes.

ment to avoid HER, suppress side reactions and possibly alleviate dendrite growth. Choline chloride (ChCl)-based DESs have received much attention among researchers since ChCl has the advantages of low cost and a scalable one-pot fabrication process, together with similar physical properties as in traditional ILs [53]. The systems normally contain Ch^+ with asymmetrical structure and complex anions composed of Cl^- and hydrogen bond donors (*i.e.*, urea, sugar, glycerin, *etc.*). In the past decade, the electrochemical deposition of Zn in ChCl-based DESs has been intensively investigated. In different ChCl-based DESs with $ZnCl_2$ as supporting salt, the viscosity of the ChCl/2urea system decreased while that of ChCl/2EG (ethylene glycol) remained similar after the introduction of $ZnCl_2$ [54]. Additionally, the extended X-ray absorption fine structure (EXAFS) results showed that the solvation structure of Zn ions in both electrolytes is identical, Zn^{2+} surrounded by four Cl^- ($[ZnCl_4]^{2-}$). However, the deposited Zn in ChCl/2urea appeared as rice grain shape (Figure 4a) while they were thin flakes in ChCl/2EG with the plates perpendicular to the electrode surface (Figure 4b). The different Zn deposition morphology can likely arise from speciation of solvated Zn ions, mass transport and double layer structure at the interface. After thorough examination of the electrolytes and the deposition behaviour in these electrolytes, they found that double-layer differences are the most likely cause of the difference. The specific adsorption of some species, presumably chloride ions, on the electrode surface prevents growth on certain faces. This result shows that not only the mass transport and solvation structure of Zn ions, but also the double layer structure at the interface plays important roles in altering the deposition behavior of Zn, which will be explained detailly in later section.

Recently, Zhi's group [55] prepared a traditional pure IL-based electrolyte, which consists of $[EMIM]BF_4$ and a supporting zinc salt $Zn(BF_4)_2$ to study the electrochemical performance of Zn metal anodes in water-free environments. In this proposed electrolyte, each Zn ion was solvated by three BF_4^- anions (Figure 4c), which facilitated the transformation of Zn^{2+} to Zn^0 via a 2D diffusion rate (Figure 4d). The ESW of the prepared IL-based electrolyte expanded to −0.75–2.8 V *vs.* Zn/Zn^{2+} (Figure 4e). By sharp contrast, the uneven Zn deposition process in aqueous electrolyte (2 M $Zn(BF_4)_2$) was unceasingly interfered with by severe side reactions (Figure 4f, g), including HER and Zn corrosion owing to the existence of detrimental water molecules. The water-free electrolyte provides a fundamental solution to the problems of HER and zinc dendrite growth in Zn-ion batteries (Figure 4h).

In the absence of water molecules, zinc ions coordinate with anions in the electrolyte rather than forming $Zn(H_2O)_6^{2+}$ complexes. These cation-anion contact ion pairs (CIPs) facilitate uniform zinc deposition through two-dimensional diffusion and promote den-

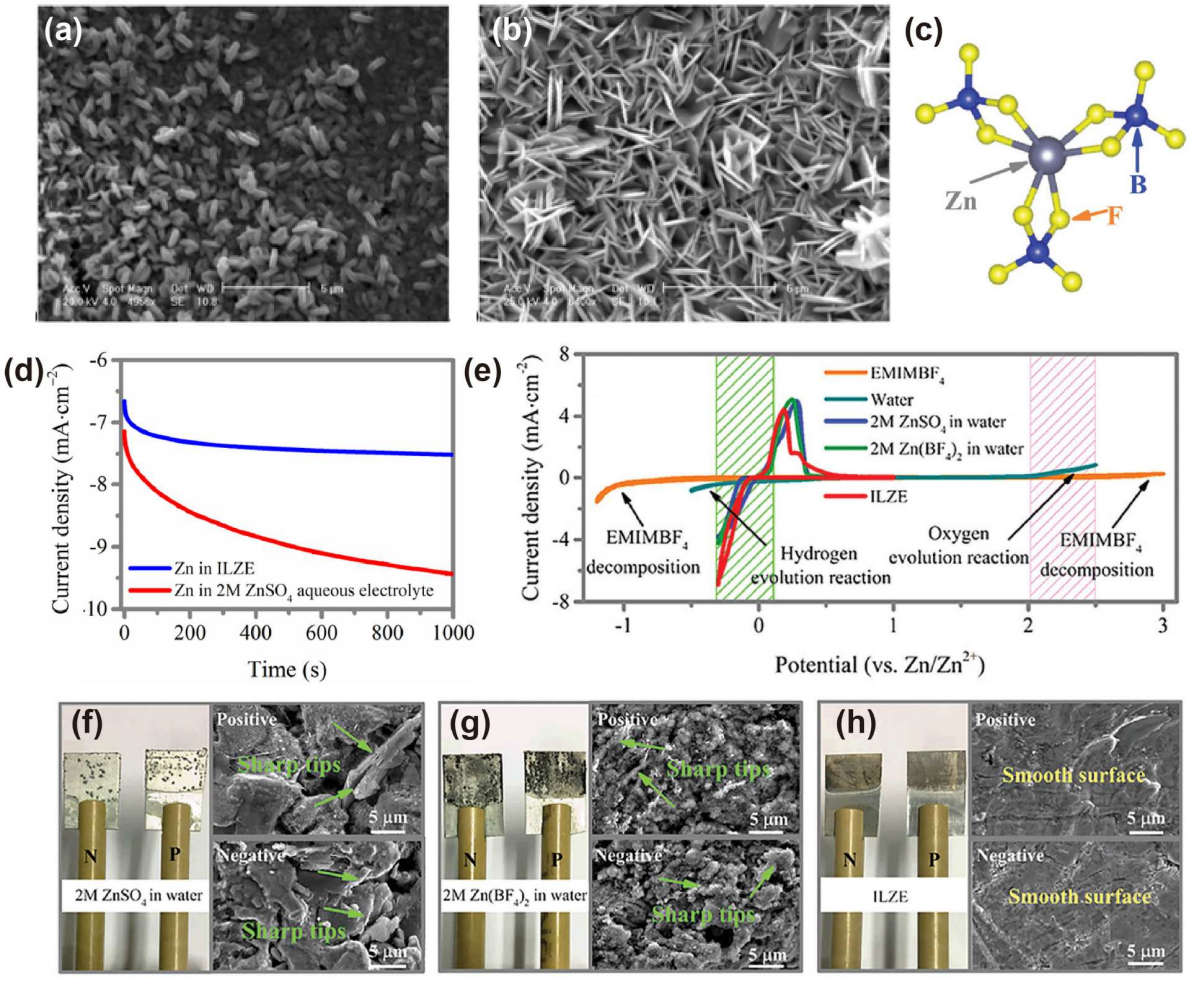

Figure 4 (Color online) Scanning electronic microscopy images of Zn deposits in (a) ChCl/2urea and (b) ChCl/2EG-based electrolytes at a current density of 3 mA cm^{-2}. Reproduced with permission from Ref. [54]. Copyright©2011, the Royal Society of Chemistry. (c) Solvation structure of Zn^{2+} surrounded by three BF_4^- in 2 M $ZnBF_4$/$[EMIM]BF_4$ electrolyte. (d) Chronoamperometry curves of Zn foils in 2 M $ZnSO_4$ aqueous electrolyte and 2 M $ZnBF_4$/$[EMIM]BF_4$ electrolyte at the overpotential of −150 mV. (e) ESW of water solvent and $[EMIM]BF_4$ IL; and cyclic voltammetry curves of Zn plating/stripping curves in different electrolytes with 3-electrode cells (Zn as both counter and reference electrode and stainless steel as working electrode). (f–h) The morphology of Zn electrodes cycled in different electrolytes after 300 cycles at a current density of 0.5 mA cm^{-2}. Reproduced with permission from Ref. [55]. Copyright©2020, Wiley-VCH.

drite-free growth of zinc anodes. Additionally, the combination of CIPs elevates the reduction potential of the anions, thereby enhancing the feasibility of forming SEI and further suppressing side reactions.

3.2 IL as supporting salt or functional additives

Even though neat IL with a supporting zinc salt can provide a water-free environment to prevent serious adverse reactions and HER, several challenges remain as follows. (i) The inherent low ionic conductivity and high viscosity compared to traditional aqueous electrolytes ($\approx 10^2$ mS m^{-1}) lead to inferior rate capability, especially at low temperatures [56]. (ii) The high cost of ILs poses a great challenge to the practical application of zinc metal batteries. Thus, incorporating ILs as supporting salts or additives in the electrolytes would be an ideal solution to overcome the above issues and bring some new benefits from ILs. To balance performance and practicality, IL-water mixed systems regulate zinc-ion solvation structures while retaining aqueous conductivity.

Zhang's group [57] reported an IL-based aqueous electrolyte with excellent anti-freezing ability by including 0.5 M [BMIM]OTF in 3 M $Zn(OTF)_2$. For example, the as-prepared electrolyte has a high ionic conductivity of 27.7 mS cm^{-1} at an extreme temperature of −40 °C while 3 M $Zn(OTF)_2$ only possess 1.28 mS cm^{-1}. The abundant hydrophilic OTF^- anions, together with big-size [BMIM] cations exhibiting a quite low binding energy with H_2O (Figure 5a), could reduce the freezing point of the IL-based electrolyte down to −62 °C by interrupting continuous H-bond networks between water molecules (Figure 5b). As a result, the $H_{11}Al_2V_6O_{23.2}$ cathode could deliver a high capacity of 160.5 mAh g^{-1} at −30 °C and exhibit excellent cyclability (Figure 5c). The disruption of hydrogen bonds was further demonstrated by the O–H stretching bands of water in the Raman and FTIR spectra (Figure 5d, e). Additionally, a higher concentration of OTF^- in the electrolyte would enhance the interactions with Zn^{2+}, thus excluding more water molecules from the inner solvation shell. To further reduce the freezing point of the electrolytes, EG, commonly used as an anti-freezing agent, was introduced as a cosolvent in IL-based aqueous electrolyte by Wang *et al.* [58]. The room-temperature liquid Zn salt is called as Zn coordinated IL (*i.e.*, $[EMIM]_5Zn(OTF)_7$), prepared by mixing the [EMIM]OTF IL with $Zn(OTF)_2$ salt in a molar ratio of 5:1. In traditional 2 M $ZnSO_4$ electrolyte, Zn^{2+} is primarily solvated by 5.2

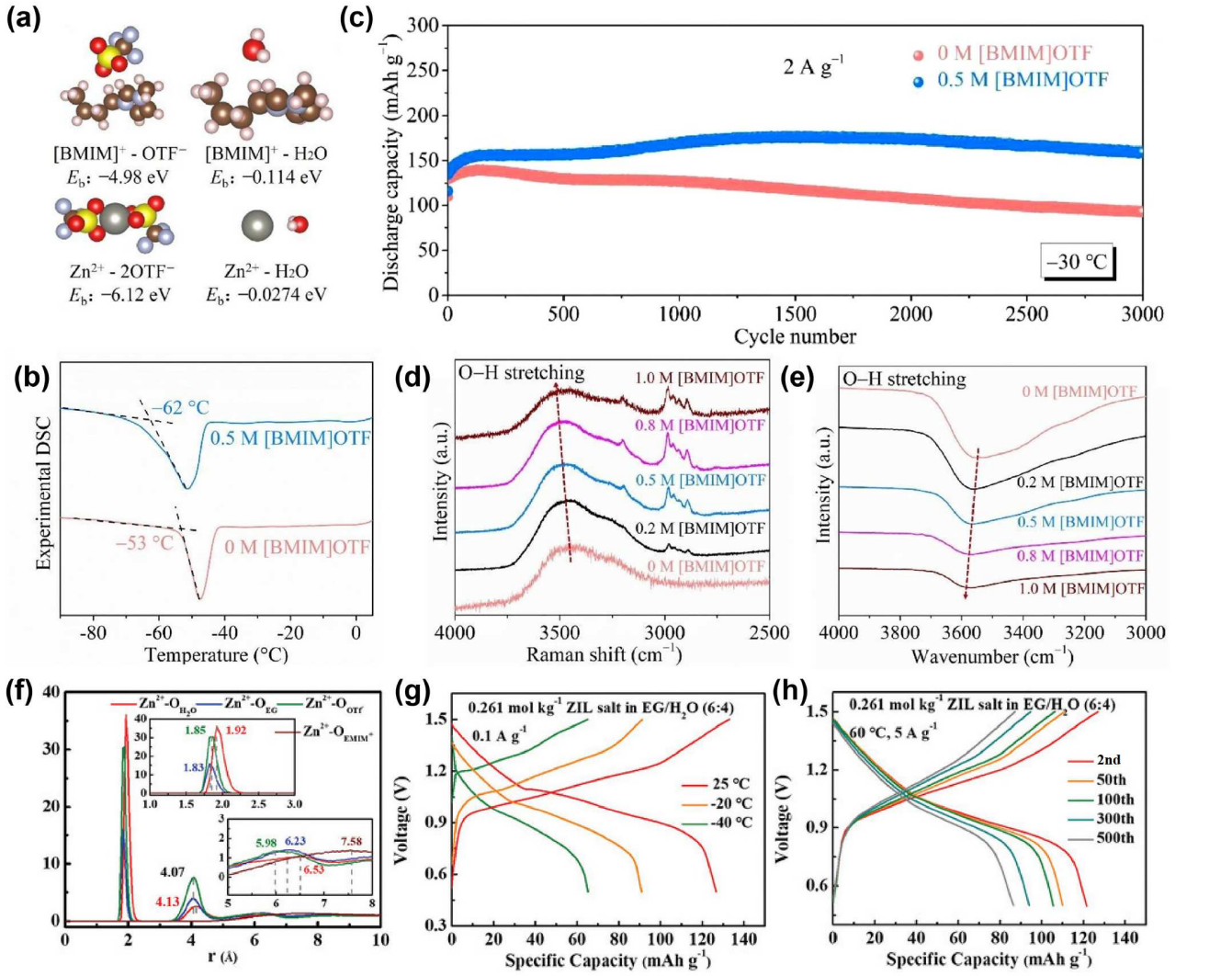

Figure 5 (Color online) (a) Binding energies of different couples. (b) Differential scanning calorimetry curves of 3 M $Zn(OTF)_2$ electrolyte with or without 0.5 M [BMIM]OTF. (c) Long-term cycling stability of Zn||$H_{11}Al_2V_6O_{23.2}$ full cells in aqueous electrolytes with/without 0.5 m [BMIM]OTF addition at −30 °C under a current density of 2 A g^{-1}. (d) Raman and (e) Fourier transform infrared (FTIR) spectra of 3 M $Zn(OTF)_2$ electrolyte with different concentrations of [BMIM]OTF. Reproduced with permission from Ref. [57]. Copyright©2022, Elsevier. (f) Radical distribution functions (RDF) of the proposed electrolyte ($[EMIM]_5Zn(OTF)_7$ in EG/H_2O mixtures) from molecular dynamics (MD). Galvanostatic charge/discharge profiles of Zn||Polyaniline cells tested (g) at different temperature with a current density of 0.1 A g^{-1} and (h) at 60 °C with 5 A g^{-1}, respectively. Reproduced with permission from Ref. [58]. Copyright©2024, Wiley-VCH.

water molecules and 0.8 SO_4^{2-} on average. These high-content solvating water molecules decompose competitively during zinc plating and stripping processes, leading to severe side reactions such as corrosion and the formation of byproducts. In contrast, the primary solvation shell of designed hybrid electrolyte largely composed of OTF^- anions and EG molecules, thus repelling water out of the inner solvation sheath (Figure 5f). Meanwhile, imidazole cations and EG molecules are crowded out of the outer solvation layer as well and interrupts H-bonds networks of water molecules, lowering the electrolyte's freezing point to below −100 °C. Additionally, thanks to the chemically ultra-stable IL and organic cosolvent, Zn||Polyaniline full cells with the designed electrolyte exhibits superior performance over a wide temperature range of −40 °C to 60 °C (Figure 5g, h), indicating strong potential for practical applications. Even though traditional $[EMIM]^+$ cations have a positive effect of unifying Zn^{2+} flux at the anode/electrolyte interface, they normally lack polar functional groups that can coordinate Zn^{2+}. Hence, Ciucci's group [30] proposed hydroxyl-functionalized [EMIM]OTF (denoted as HO-Emim) working as a bi-functional electrolyte modulator for AZMBs. In $[EMIM]^+$-contained electrolyte, the [EMIM] cation didn't show up in the first solvation shell of Zn^{2+}. Oppositely, in the presence of HO-Emim, the obvious HO-Emim signal appeared in the primary solvation sheath as shown in Figure 6a–c. Accordingly, the coordination number of water molecules in the inner solvation sheath gradually reduced. There are 5.09 water molecules in standard 2 m $Zn(OTF)_2$ electrolyte and 5.01 water molecules in [EMIM]-based electrolyte because of higher OTF^- population. Notably, only 4.90 water molecules were present in the HO-Emim incorporated electrolyte, suggesting that HO-Emim will further break the hydrated Zn^{2+} shell by partially replacing water molecules. This result underscores the highly tailorable structure of ILs and their versatility for a wide range of application scenarios.

Similarly, IL ([EMIM]OAc, denoted as EAc) with another hydrophilic anions were introduced to a 2 M $ZnSO_4$ electrolyte, effectively altering the solvation structure of Zn^{2+} [59]. Notably, OAc^- not only have strong interactions with water molecules via H-bonds formation because of their hydrophilic feature, but also exhibit excellent solvation affinity to Zn^{2+} [50,60]. The MD and spectroscopy results confirmed that the solvation structure composition changed by EAc. Specifically, EAc mainly increased the CIP of Zn^{2+}–SO_4^{2-} from 17.8% to 26.6% (Figure 6d). In addition, acetate anions entered the first solvation shell as well and increased Zn^{2+}–OAc^- CIPs. Therefore, the solvated water content is comparatively reduced in IL-modified electrolyte, which is beneficial to suppressing side reactions related to water activity [49]. In addition, the altered water activity in the bulk electrolyte was confirmed by Raman results in Figure 6e. Interestingly, [EMIM]FSI, a water-immiscible IL, was utilized to enable stable and environment-adaptable AZMBs as well [42]. Initially, 1 m [EMIM]FSI was immiscible with water, forming a biphasic mixture. After adding 3 m $Zn(OTF)_2$ to the binary mixture, the ternary system formed a clear, homogeneous solution (Figure 6f). This distinct miscibility transition allows for the separation and subsequent recycling of high-value components from the electrolyte through a mild drying process, facilitated by the near-zero vapor pressure feature of the IL. According to the MD simulations, $Zn(OTf)_2/H_2O$-[EMIM]FSI has a more negative interaction energy compared to H_2O-EmimFSI, explaining the miscibility transition phenomenon of the ternary systems. From a physicochemical perspective, the coexistence of the hydrophobic $–CF_3$ group and the hydrophilic sulfonate group ($–SO_3$) within the OTf^- anion imparts an amphiphilic nature to $Zn(OTf)_2$, enabling it to modulate the miscibility between two or more solvents with differing hydrophobicity. At the molecular scale, the IL works as a "water pocket" to significantly suppress water activity (Figure 6g), attributed to enclosing highly active H_2O-dominated Zn^{2+} complexes to protect them from parasitic reactions due to the weak solvating capability of [EMIM]FSI. Alternatively, ILs as additives introduce interfacial stabilization and dendrite suppression at low dosage, offering a cost-effective solution. Shen *et al.* [61] added 1% of $[BMIM]PF_6$ as a multifunctional IL additive to the base electrolyte (2 M $ZnSO_4$). Despite the smaller dosage, the downshift of the O–H stretching vibration from 3172.2 to 3116.7 cm^{-1} with increasing $[BMIM]PF_6$ concentration (from 1% to 10%) indicates effective modulation of the H-bonding network (Figure 6h). The $[BMIM]PF_6$ was confirmed to alter the solvation structure of Zn^{2+} by simulation results. 0.12 PF_6^- molecules entered the inner solvation shell of Zn^{2+} by replacing water molecules (Figure 6i, j). Additionally, [BMIM] cations have strong interactions with sulfate anions (Figure 6k), therefore suppressing the formation of $Zn_4SO_4(OH)_6{\cdot}xH_2O$ as a by-product, which is consistent with the fact that the suppressed Zn corrosion after immersion in IL-added electrolytes is characterized by *ex-situ* XRD measurements. Table 2 summarizes the diverse applications of ILs employed as supporting salts or additives in AZMBs.

While various ILs have been explored for AZMBs, imidazolium-based ILs are among the most frequently studied in this field. More broadly, imidazolium-based ILs also represent the most extensively investigated and data-rich category of ILs across multiple research areas [72]. Specifically, with appropriate alkyl chain lengths (*e.g.*, [BMIM]OTF), they typically exhibit low melting points, low viscosity, and high ionic conductivity. These properties make them more suitable than other types of ILs for applications in AZMBs, which require electrolytes with superior electrochemical performance. For instance, the electrolyte composed of 3 M $Zn(OTF)_2$ with 0.5 M [BMIM]OTF shows only a 5.8% decrease in ionic conductivity compared to the base electrolyte while exhibiting excellent anti-freezing performance [57]. In contrast, adding 0.5 M trimethylethyl ammonium-OTF to a 4 M $Zn(OTF)_2$ aqueous solution leads to an 18.2% reduction in ionic conductivity, with almost no improvement in anti-freezing capability [73]. Despite these advantages, imidazolium-based ILs indeed have notable limitations. Their synthesis, especially with fluorinated anions, is often costly, limiting large-scale use. Environmental and toxicity concerns still exist, as many of them exhibit poor biodegradability. Besides, their long-term stability can be compromised under harsh electrochemical conditions. Therefore, their practical application requires balanced performance with cost, sustainability, and durability for achieving excellent task-specific materials.

3.3 ILs composite-based gel electrolytes

Furthermore, IL-based gel electrolytes integrate mechanical robustness with ionic conductivity and flexibility.

As an ideal polymer matrix, polyacrylamide (PAM) exhibits stable physicochemical properties, suitable swelling behavior, and excellent flexibility, owing to the hydrogen bonding between its polymer chains and water molecules [74]. However, conventional $PAM/ZnSO_4$ systems still encounter drawbacks such as low ionic conductivity, side reactions with zinc, and zinc dendrite formation, which degrade battery performance and limit their application [74]. ILs have advantages of wide ESW, high ionic conductivity and adjustable structures. For instance, the ILs that have imidazole cations and hydrophilic anions could effectively suppress HER, thus prolonging battery lifespan. In addition, IL can form a stable solvation structure to reduce solvated water content, suppress free-water activity and dendrite formation. In this regard, introducing ILs into the PAM-based hydrogel offers a way to strike a balance

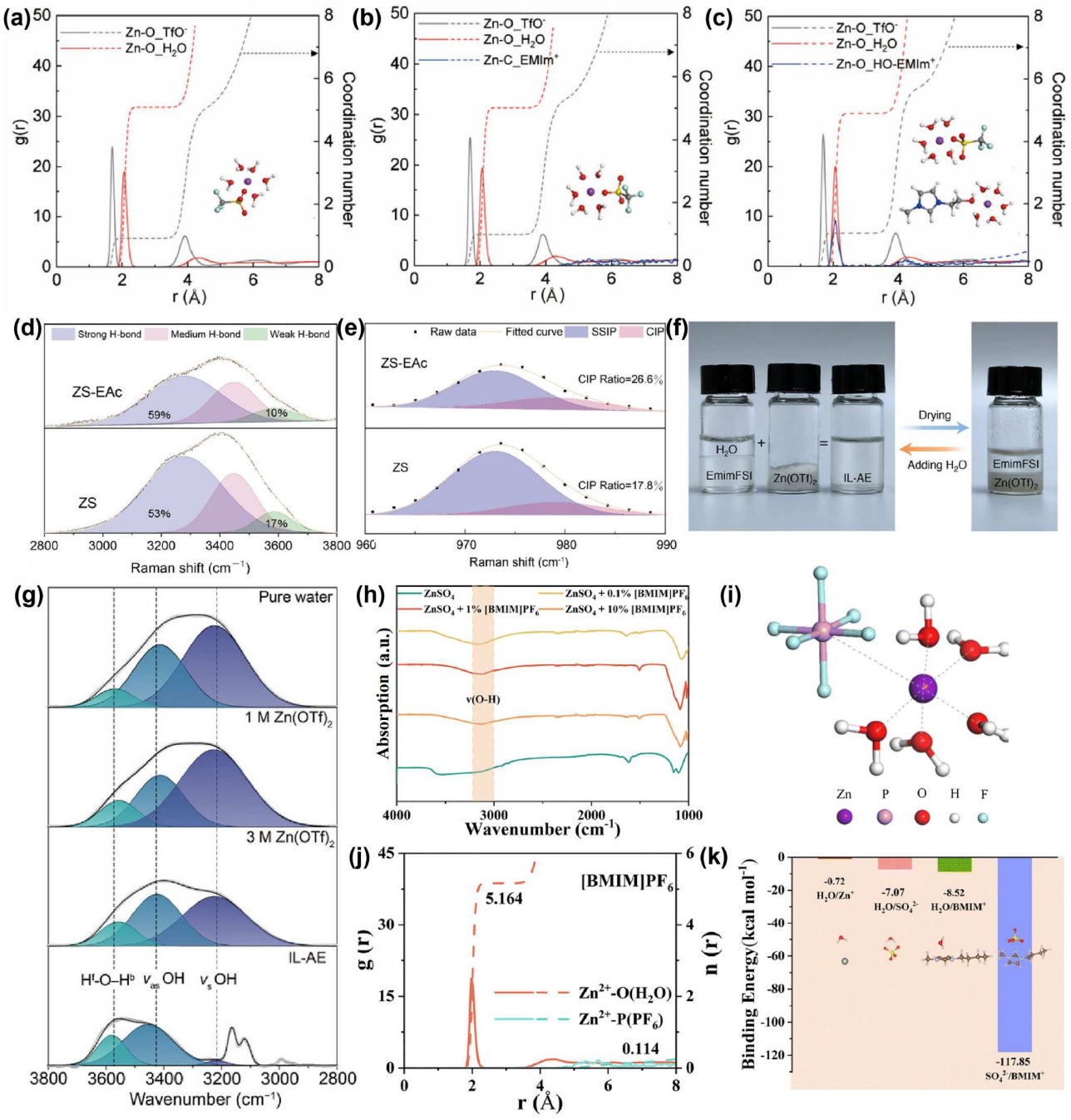

Figure 6 (Color online) RDFs of (a) 2 m $Zn(OTF)_2$, (b) 2 m $Zn(OTF)_2$ with [EMIM]OTF IL, and (c) 2 m $Zn(TfO)_2$ with HO-[EMIM]OTF IL, respectively. Reproduced with permission from Ref. [30]. Copyright©2025, Wiley-VCH. Raman spectra fitting at the region of (d) 2800–3800 cm^{-1} and (e) 960–990 cm^{-1} of different electrolytes for analyzing the H-bond structure and CIP statistical results, respectively. Reproduced with permission from Ref. [59]. Copyright©2024, Wiley-VCH. (f) Optical images show that addition of $Zn(OTf)_2$ transforms the immiscible H_2O-[EMIM]FSI mixture into a homogeneous solution. (g) Attenuated total reflection FTIR spectra of O–H stretching in the region from 3800 to 2800 cm^{-1} for pure water, 1 M $Zn(OTf)_2$, 3 M $Zn(OTf)_2$, and $Zn(OTf)_2/H_2O$-EmimFSI electrolyte. Reproduced with permission from Ref. [42]. Copyright©2023, Wiley-VCH. (h) FTIR spectra of 2 M $ZnSO_4$ and electrolytes with different doping concentrations of $[BMIM]PF_6$ additive. (i) Representative solvation structure and (j) RDFs of electrolyte with $[BMIM]PF_6$ additive obtained from MD simulations. (k) The binding energies of H_2O/Zn^{2+}, H_2O/SO_4^{2-}, $H_2O/BMIM^+$, and $SO_4^{2-}/BMIM^+$ couples. Reproduced with permission from Ref. [61]. Copyright©2025, the Royal Society of Chemistry.

between mechanical strength, ionic conductivity, and battery performance [75,76]. Accordingly, Chen's group [77] prepared a hybrid hydrogel electrolyte (denoted as PDEM), including a PAM network, $ZnSO_4$, $[EMIM]BF_4$, and DES (mixture of $ZnClO_4$ and EG) based on the characteristics of DES and IL (Figure 7a). The F atom in the BF_4 anion not only forms strong H-bonds with multiple functional groups, like hydroxyl, amino, EG, *etc.*, but also has weak interactions with cations (*e.g.*, hydrated Zn^{2+}). These features allow for the sustainment of weak cross-linking during deformation, thus significantly enhancing the deformation ability of polymer networks. Meanwhile, the polar groups of IL strengthened the interactions with free water, improving anti-freezing resistance. Besides the introduction of ILs, Zhang *et al.* [78] incorporated 2,2,6,6-tetramethylpiperidine-1-oxyl-oxidized bacterial cellulose (denoted as TBC) into the PAM-based hydrogel to prepare dual-crosslinked polymer networks. A 2 M $ZnSO_4$ aqueous electrolyte was utilized as a comparison (Figure 7b). The composition of the proposed hydrogel electrolyte was presented in Figure 7c,

Table 2 Recent developments of the electrochemical performance of Zn anodes in aqueous electrolytes incorporating IL as supporting salts or additives

Electrolyte composition	Main functions	Average CE (%)	Cycling lifespan	Ref.
3 M $Zn(OTF)_2$ + 0.5 M [BMIM]OTF	Promoting SEI formation H-bonds modulation	99.46	500 h (5, 25)	[57]
20 wt% H_2O + 100 wt% $Zn_{0.5}$[BMIM]$(TFSI)_2$	H-bonds modulation Promoting SEI formation	99.27	1000 h (1, 0.5)	[62]
3 M $Zn(OTF)_2$ + 1 M [EMIM]FSI	Regulating SEI formation Solvation structure reconstruction	Over 99	680 (1, 1)	[42]
1 M $ZnSO_4$ + 1 wt% $[DMP]BF_4$[a)]	H-bonds modulation Promoting SEI formation Solvation structure reconstruction	97	1400 h (5, 2.5)	[63]
2 M $ZnSO_4$ + 0.2 M [EMIM][OAc]	EDL reconstruction Solvation structure altering H-bonds modulation	Over 99	1000 h (10, 10)	[59]
0.261 M $(EMIM)_5Zn(OTF)_7$ in EG:H_2O (6:4)	Solvation structure altering H-bonds modulation Promoting SEI formation	Over 99	2500 (1, 1)	[58]
3 M $Zn(OTF)_2$ + 1 M [EMIM]FSI	Solvation structure altering H-bonds modulation Promoting SEI formation	Over 99	2000 (1, 1)	[64]
$Zn(BF_4)_2$:$EMIMBF_4$ = 1:3 (molar ratio)	Regulating SEI formation Solvation structure altering	99.73	1300 (1, 1)	[65]
2 M $ZnSO_4$ + 1% $[BMIM]PF_6$	Solvation structure altering EDL reconstruction	99.87	1000 (4, 0.5)	[61]
1 M $ZnSO_4$ + 0.05 M $[EMIM]BF_4$ or [EMIM]Ts	H-bonds modulation at the interface	Over 99	Over 1000 h (1, 0.5)	[51]
2 M $ZnSO_4$ + 0.1 M [EMIM][OAc]	EDL reconstruction Solvation structure altering H-bonds modulation	99.65	Over 2000 h (5, 1)	[33]
1 M $ZnAc_2$ + 0.1 M [EMIM][Ac]	Solvation structure altering EDL reconstruction	–	1350 h (1, 1)	[66]
2 M $ZnSO_4$ + 0.025 M $[BMIM]HSO_4$	EDL reconstruction	99.5	5310 h (1, 1)	[67]
$Zn(OTF)_2$:[EMIM]OTF:H_2O = 6:10.8:0.056 (molar ratio)	EDL reconstruction Promoting SEI formation Solvation structure altering	98.8	3400 h (2, 2)	[68]
2 M $ZnSO_4$ + 0.2 M [EMIM]OTF	Solvation structure altering Regulating SEI formation EDL reconstruction	99.6	900 (5, 5)	[69]
2 M $Zn(OTF)_2$ + 0.6 M HO-[EMIM]OTF	Solvation structure altering	99.6	1800 h (1, –)	[30]
0.5 M $ZnCl_2$ + 1 M [EMIM]I	Solvation structure altering Promoting SEI formation	–	592, (5, 2.5)	[70]
2 M $ZnSO_4$ + 0.05 M [BMIM]Br	Solvation structure altering Regulating SEI formation EDL reconstruction	99.42	2700 (1, 1)	[71]

a) $[DMP]^+$ is the abbreviation of *N*,*N*-dimethylpyrrolidinium cation.

demonstrating a three-dimensional network connection. This dual-crosslinked polymer hydrogel enables high ionic conductivity of 43.7 mS cm^{-1} and brilliant mechanical strength (tensile strength: 175.25 kPa; elastic modulus: 3.48 GPa; elongation at break: 38.36%). Furthermore, the –COOH and $–CONH_2$ functional groups on the crosslinked networks, together with the BF_4^- anions, can coordinate with Zn^{2+}. This coordination modulates the Zn^{2+} solvation structure and reduces the nucleation overpotential during deposition.

Recently, Zhang's group [79] introduced [EMIM]OAc to polyvinyl alcohol (PVA)-based hydrogel to decrease water activity and enhance low-temperature durability (Figure 7d). $[EMIM]^+$ can have stronger interactions with the chain segments of PVA rather than water molecules by forming H-bonds, leading to abundant crystalline microregions and facilitating physical cross-linking. As a result, these crystalline sites gradually enhanced the mechanical strength (*i.e.*, 0.28 MPa of fracture strength and 362.78% of fracture strain) of hydrogel electrolyte (Figure 7e). Additionally, by comparing the binding energies of different species in Figure 7f, it indicates that water molecules primarily interact with PVA and $[EMIM]^+$ rather than H_2O, thus disrupting continuous H-bonds network between water molecules (Figure 7f). Meanwhile, Li's group [80] designed a supramolecular IL gel electrolyte consisting of PVA polymer matrix and $[BMIM][ZnBr_3]$ IL, which exhibits remarkable mechanical properties, including a tensile strength of 2.22 MPa, a deformation capability exceeding 1200%, and a high toughness of 1900.74 MJ m^3. Thanks to its unique stress dissipation mechanism, the anode achieves an extended cycle life of over 2000 h. The above-mentioned results prove that the integration of IL into the hydrogel electrolyte would provide more abundant interactions between species within the gel electrolyte and bring excellent mechanical properties.

3.4 Polymerized ILs

Finally, polymeric ILs extend the concept by immobilizing IL moieties within polymer matrices, enabling stable ion transport networks and improved electrochemical stability. Recently, Liu's group [81] designed zwitterionic poly-IL hydrogel electrolyte (PICZ) for flexible AZMBs. The cation of 1-carboxymethyl-3-vinylimidazolium bromide (CAVIm) IL was grafted onto the PAM backbone (Figure 8a). Besides, chitosan (CS) was also introduced to the

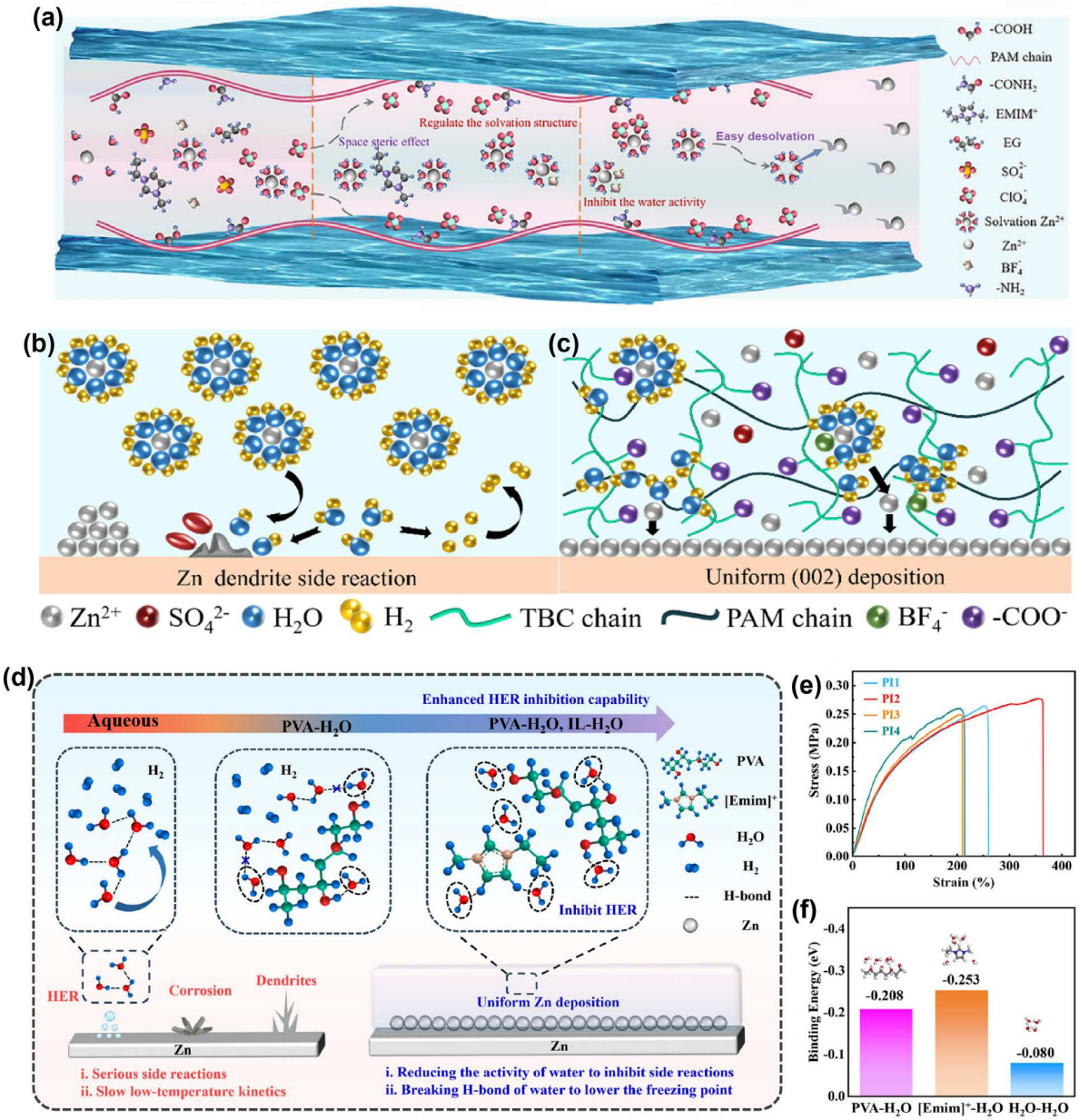

Figure 7 (Color online) (a) The schematic illustration of the molecular motion inside the PDEM electrolyte. Reproduced with permission from Ref. [77]. Copyright©2025, Wiley-VCH. (b, c) Schematic illustration of the solvation structure and interfacial activities in different electrolytes. Reproduced with permission from Ref. [78]. Copyright, 2024, Elsevier. (d) Schematic illustration of the anti-freezing and side-reaction suppression mechanisms in the as-prepared PVA-IL hydrogel electrolyte. (e) Mechanical properties of different hydrogels. (f) The binding energies of PVA-H_2O, $[EMIM]^+$-H_2O, and H_2O–H_2O. Reproduced with permission from Ref. [79]. Copyright©2025, Wiley-VCH.

hydrogel electrolyte and interacted with CAVIm, improving the ionic conductivity and mechanical strength by formation of protonated amines and carboxylate anions. The unique structure of profound immobilized cations/anions (imidazole cation, $–COO^-$ and $–NH_3^+$) within the system enables fast ions diffusion under electric field, leading to high ionic conductivity of 25.62 mS cm^{-1}. MD simulation was employed to study the characteristics of PICZ. The RDFs show that the Zn–O (CAVIm) is 1.98 Å while Zn–O (OTf^-), Zn–O (H_2O), and Zn–O (AM) are all 2.03 Å (Figure 8b, c), indicating that carboxylate anions, acyl group and triflate anions can all solvate with Zn ions. From the statistic results, the coordination number of each zinc ion is six, including 0.1 CAVIm, 0.28 AM, 0.32 OTF^-, and 5.3 water molecules, substituting partial water from $Zn(H_2O)_6^{2+}$ complexes in traditional diluted electrolyte. Furthermore, the Raman results gave an overview of modified water activity after adding CAVIm and CS, allowing for reduced corrosion and side reactions. Chen *et al.* [31] grafted imidazole-based IL onto esterified cellulose to design polymerized IL as well but employed the cellulose-based poly-IL as electrolyte additive (Figure 8d). Cellulose intrinsically has many H-bonds formation sites on its backbone, like –OH and ether oxygen atom. The feature of imidazole-based IL is the imidazole ring, which can be involved into nitrogen or protons induced H-bonds. Even though big-size IL cations can play roles in homogenizing the electric field at the Zn/electrolyte interface and promote uniform Zn deposition, traditional quaternary ammonium cations lack the ability to further regulate H-bonds of the electrolytes compared to imidazole-based IL. Therefore, the proposed cellulose-based poly-IL additive exhibits significant synergetic H-bonds reconstruction and ion regulation capability towards AZMBs. Similarly, Xu *et al.* [82] designed CS-based poly(aprotic/protic IL)s through Brønsted acid-base reaction utilized as additive to modulate the local chemical environment at electrode/electrolyte

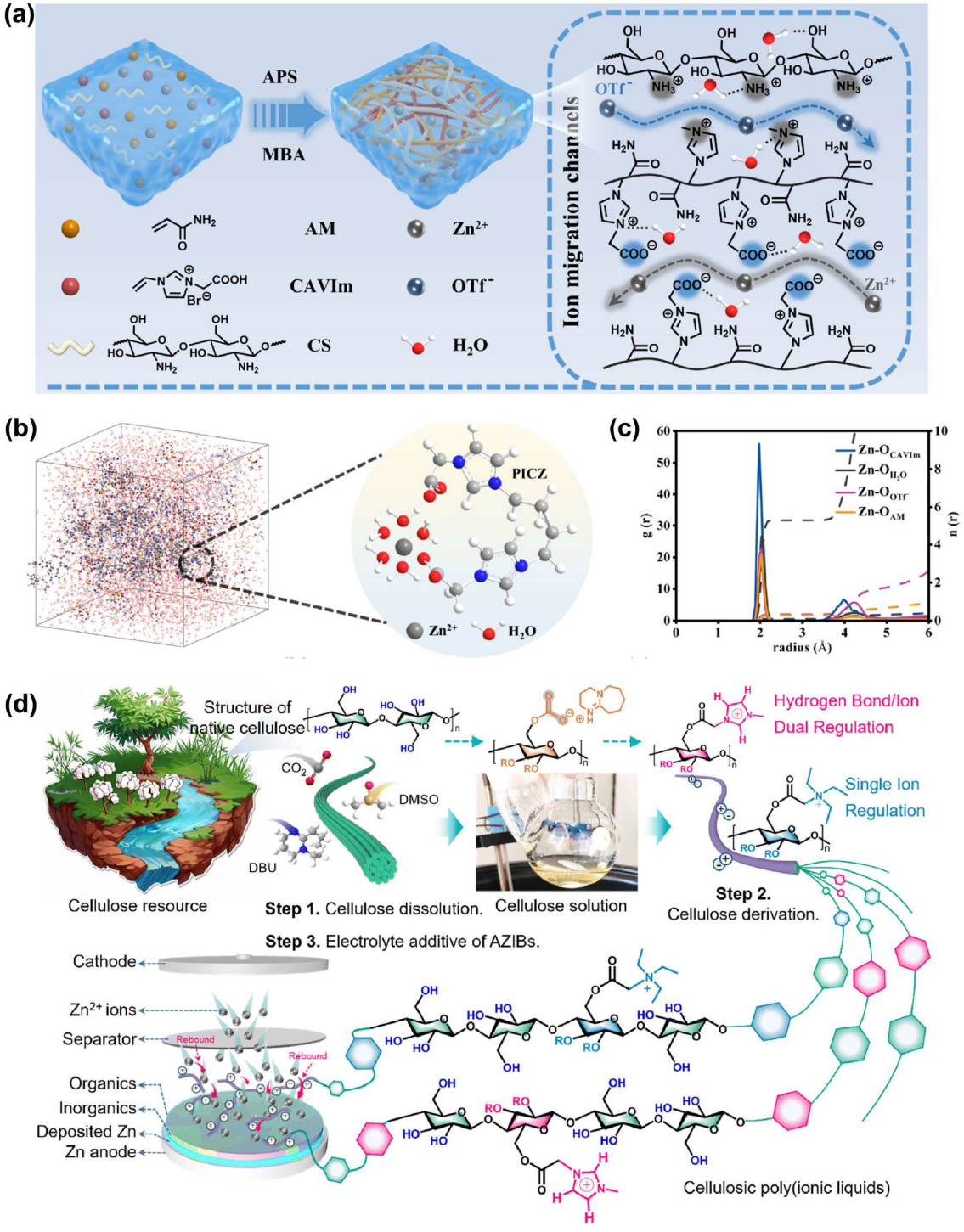

Figure 8 (Color online) (a) Schematic diagram of the composition and interactions of PICZ gel electrolyte. (b) Snapshot and (c) RDFs of PICZ electrolyte during MD simulations. Reproduced with permission from Ref. [81]. Copyright©2025, Elsevier. (d) Schematic illustration for the preparation of the cellulosic PIL electrolyte additive. Reproduced with permission from Ref. [31]. Copyright©2025, the Royal Society of Chemistry.

interface and cation-anion interactions in the electrolyte.

4 IL-induced interfacial engineering

The parasitic reactions, like HER, corrosion, coupled with uncontrolled dendrite formation, originate from the chaotic interfacial environment at the Zn/electrolyte interface [2]. Since the structure of the bulk electrolyte and the interfacial properties are intrinsically linked, the components, compositions, solvation structure and interactions of different species within the electrolytes directly determine what will happen on the interface. Therefore, IL-based effective electrolyte engineering will promote ideal interfacial chemistry on two critical factors by inhibiting side reactions and dendrite growth. One key strategy involves modulating the structure and composition of the EDL to guide Zn^{2+} desolvation and transport. This is achieved as the bulky cations from the IL adsorb onto the Zn surface, which helps mitigate the tip effect during zinc deposition (promoting uniform deposition). Concurrently, this cation adsorption displaces water molecules from the interface, creating a water-poor local environment that effectively

suppresses parasitic side reactions. On the other hand, IL-altered solvation structure possesses reduced water molecules coordinated to Zn^{2+}, thereby making the HER less favorable. Additionally, this modified solvation environment increases the likelihood of anion reduction, which promotes the *in-situ* formation of a robust and Zn^{2+}-conductive SEI. This SEI further inhibits side reactions and contributes to more uniform zinc deposition. Therefore, this section will delve into these fundamental mechanisms, exploring how IL-based electrolytes induce EDL restructuring and derived SEI formation are pivotal in unlocking the full potential of durable zinc metal anodes.

4.1 EDL modulation at Zn anode surface

The interface is the boundary located between two substances or the same substance with different physical states, also called a phase boundary [83]. In AZMBs, the interface refers to the phase boundary between the electrodes and the electrolyte. EDL formation originates from the chemical potential difference between the cathode and anode. The chemical potential of a Zn atom is associated with Zn^{2+} and electrons. Since the electrolyte is an ionic conductor, the chemical potential of Zn^{2+} in the anode, electrolyte and cathode are identical as long as the circuit is opened. Additionally, electrodes with electronic channels are isopotential [84]. Therefore, EDL formed at the interface undertakes the difference between cathode and anode, which correspondingly determines the interfacial chemistry and electronic properties. The understanding of EDL structure has evolved over 100 years. For AZMBs, the modified Gouty-Chapman-Stern and BockrisDevanathan-Müller models are widely accepted to describe the EDL structure [85]. EDL consists of a compact layer (CL) and a diffusion layer (DL). CL is further classified into the inner Helmholtz plane (IHP) and an outer Helmholtz plane (OHP), as shown in Figure 9. The EDL model precisely dictates the electrochemical process at the Zn anode interface. In a traditional dilute $ZnSO_4$ electrolyte, the primary solvation shell of Zn^{2+} comprises six water molecules, as existing in the DL and OHP. The hydrated Zn ions are bound at OHP by electrostatic interactions due to the limited space in IHP, while water molecules and SO_4^{2-} anions are located at the IHP by specific adsorption. During Zn deposition process, the $Zn(H_2O)_6^{2+}$ complexes diffuse from DL to OHP and then go through de-solvation. The naked Zn ions will be reduced and deposited on the Zn electrode by long-term electrostatic force. At the same time, H_2O will decompose into H_2 and OH^- due to the relatively low Zn/Zn^{2+} redox potential. Afterwards, the generated OH^- will rapidly interact with Zn^{2+} and SO_4^{2-} to form side products, thus causing lower CE and instability to the battery performance. Additionally, the high desolvation energy barrier will prevent smooth Zn^{2+} diffusion between OHP and IHP, resulting in uneven Zn^{2+} flux and then facilitating dendrite formation. Therefore, modulating EDL at the Zn surface is crucial to suppress parasitic reactions and dendrite formation.

As cations in ILs normally possess large sizes, they tend to adsorb on the Zn surface, thereby altering the EDL structure. Due to the significant difficulties of exploring the EDL structure at the nanoscale, simulation methods were often used to investigate and hypothesize the EDL structure. Fan's group [59] carried out MD simulations to examine the distribution of H_2O molecules and $[EMIM]^+$ near Zn surface based on the two electrolytes of 2 M $ZnSO_4$ (ZS) and 2 M $ZnSO_4$ + 0.2 M [EMIM]OAc (ZS-EAc). The snapshots of MD simulations revealed the abundance of $[EMIM]^+$ in IHP (Figure 10a). Then the distribution density of H_2O molecules and $[EMIM]^+$ further suggests that $[EMIM]^+$ repels water molecules out of IHP (Figure 10b, c). Together with the modified primary solvation structure of Zn^{2+} via OAc^- in OHP, the water content in EDL of IL-modified electrolyte reduced significantly (Figure 10d), thereby boosting the electrochemical performance of Zn anodes. Differently, Chen *et al.* [57] employed DFT method to determine the adsorption energy of different species on Zn surface as shown. The adsorption energy of $[BMIM]^+$ cations (−2.08 eV) on (002) plane of Zn anode is much more negative than that of water molecules (−0.221 eV), which means $[BMIM]^+$ cations are preferentially adsorbed on Zn surface during Zn deposition process, creating water-poor surface (Figure 10e, f). Similar results are found as well in some other literature [33,66–69,71]. Notably, hydrophobic IL, $[BMIM]PF_6$, was also introduced to adjust the EDL structure in 2 M $ZnSO_4$ electrolyte [61]. The preferential adsorption of [BMIM] cation on Zn (002) surface was confirmed by the First-principles calculation (DFT). The adsorption energy of $[BMIM]^+$ on Zn surface (−1.07 eV) is relatively low when compared to that of water molecules (−0.14 eV) (Figure 10g, h). This result suggests that [BMIM] cations exhibit higher affinity to Zn surface and rule out partial water out of IHP, thus effectively suppressing water-induced side reactions. Then, the contact angle test of the electrolytes was performed to examine the affinity between the electrode and electrolyte. The contact angle on Zn surface in bare electrolyte is 86.72° as shown in Figure 10i. After introduction of $[BMIM]PF_6$, the contact angle was reduced to 70.04°, demonstrating that $[BMIM]PF_6$ has better affinity to Zn surface, likely attributed to the

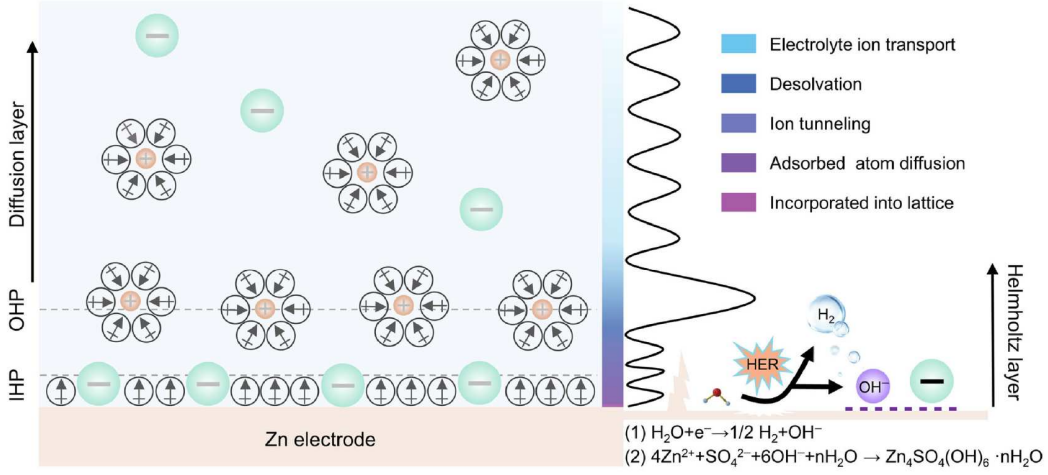

Figure 9 (Color online) Schematic diagram illustrating the structure of the EDL at a Zn electrode in aqueous $ZnSO_4$ solution. Reproduced with permission from Ref. [85]. Copyright©2023, Elsevier.

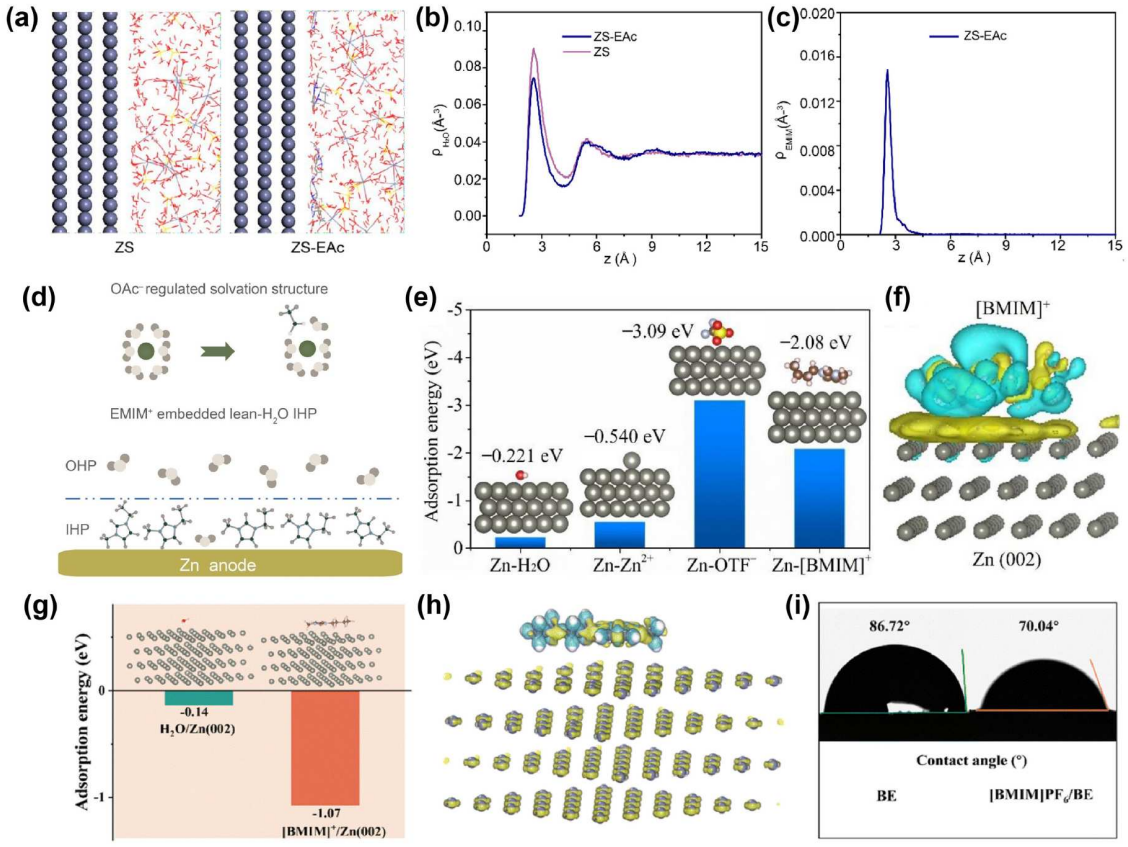

Figure 10 (Color online) (a) Snapshots of the Zn/electrolyte interface in ZS and ZS-EAc electrolytes. The distribution density of (b) water molecules and (c) EMIM cations near the Zn surface obtained from simulation results. (d) Solvation structure of Zn^{2+} and EDL structure on Zn surface in IL-modified electrolyte. Reproduced with permission from Ref. [59]. Copyright©2024, Wiley-VCH. (e) Adsorption energies of H_2O, Zn^{2+}, OTF^-, and $[BMIM]^+$ on Zn (002) surface. (f) Charge density distribution diagram for $[BMIM]^+$ adsorbed on Zn (002) surface. Electron accumulation and depletion are shown in yellow and cyan, respectively. Reproduced with permission from Ref. [57]. Copyright©2022, Elsevier. (g) Adsorption energies of water molecules and $[BMIM]^+$ on Zn (002) surface. (h) Charge density difference diagram for $[BMIM]^+$ adsorbed on Zn (002) surface. (i) Contact angle of different electrolytes on Zn electrodes. Reproduced with permission from Ref. [61]. Copyright©2025, the Royal Society of Chemistry.

preferential adsorption of [BMIM] cation on Zn surface.

Even though the cations of hydrophilic or hydrophobic IL can repel partial water molecules out of the interface by adsorbing on the Zn surface, the anions, which mainly determine the hydrophilic properties of individual IL, may play important roles in modulating hydrogen bonds at the interface as well. Sun's group [51] thoroughly investigated the influence of both hydrophilic and hydrophobic IL on the interfacial structure at the anode/electrolyte interface. In this work, they chose 1 M $ZnSO_4$ as a control group (denoted as base) and 1 M $ZnSO_4$ containing hydrophilic $[EMIM]BF_4$ (denoted as IL-philic) or hydrophobic [EMIM] *p*-toluene sulfonate (denoted as IL-phobic) as experimental groups. H-bonds between water molecules are complicated and attenuated total reflection FTIR (ATR-FTIR) was utilized to detect and analyze these H-bonds. H-bonds with different chemical environments have various vibration patterns, which can be examined through spectra deconvolution. The higher the wavenumber of the OH stretching, the weaker the H-bonds. As shown in Figure 11a, the ATR-FTIR spectra of the three bulk electrolytes at the region of OH stretching display nearly identical appearance, indicating that 0.02 m of IL addition have little impact on the H-bonds of the bulk electrolyte. However, the H-bonds environment at the anode/electrolyte interface shows the opposite, detected by SEIRAS with higher sensitivity (Figure 11b). The peakfit results show that the strong H-bonds ratio in both IL-based electrolytes increased while the weak H-bonds decreased. The increasement of strong H-bonds makes it harder for H_2O to deprotonate, consequently suppressing water activity. The schematic mechanism of this finding is illustrated in Figure 11c. Since IL cations are preferentially adsorbed on Zn surface, the anions are located at an outer area by electrostatic interactions. Specifically, for IL-philic anions, they form strong H-bonds with water molecules due to their hydrophilic property at the interface. In the case of IL-phobic anions, they repel water molecules and induce them to aggregate and form strong H-bonds. A highly refined technique is presented in this work to probe OH signals at the electrode/electrolyte interface, thereby opening new avenues for the development of highly sensitive sensing technologies.

4.2 Formation of IL-derived SEI-like layers

The concept of SEI is derived from nonaqueous lithium-ion batteries proposed by Peled in 1979 (Figure 12a) [86]. Since then, as shown in Figure 12b–d, multi-layered model, the Mosaic model and plum pudding model were brought up to describe the SEI layers in various battery systems [87]. SEI is a protective layer which prevents the continuous decomposition of electrolytes and extends the ESW of the electrolytes. A well-formed SEI not only preserves electrochemical stability under operating conditions exceeding the thermodynamic limits of the electrolyte but also improves the structural integrity of the electrode itself. Key characteristics of an optimal electrode/electrolyte interphase include: (i) high ionic conductivity coupled with effective electronic insulation; (ii) resistance to thermal and chemical degradation; (iii) a dense and homogeneous

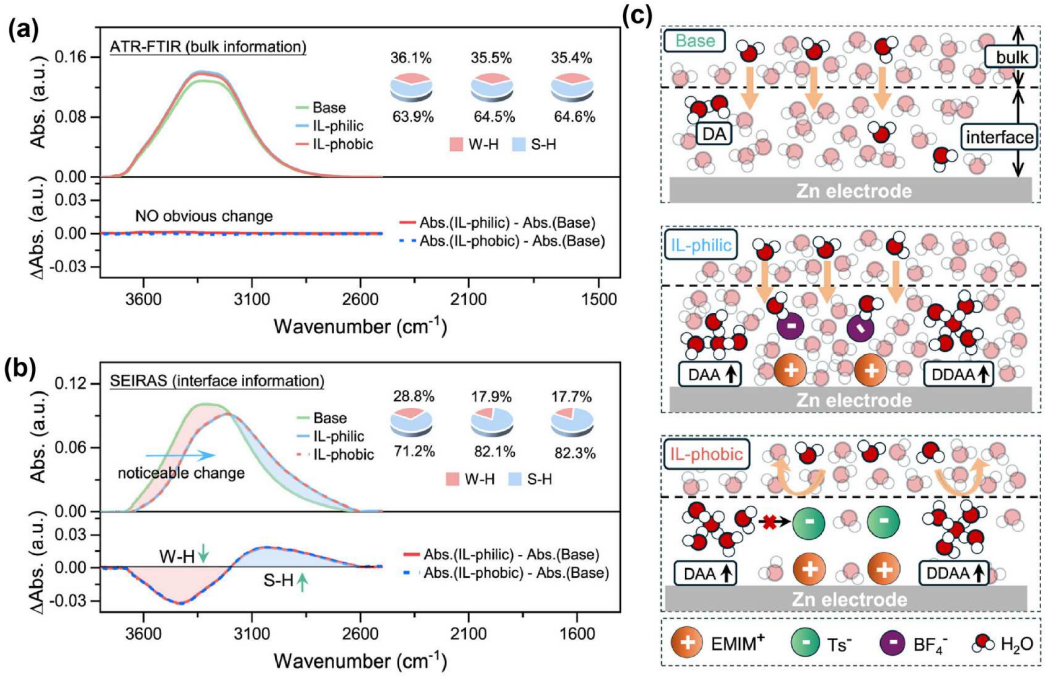

Figure 11 (Color online) (a) ATR-FTIR spectra in the regions of 3800–2600 cm^{-1} and distributions of strong and weak H-bonds of the bulk electrolytes (top). The bottom is the corresponding difference spectra. (b) Surface-enhanced infrared absorption spectroscopy (SEIRAS) spectra and strong and weak H-bond contents for the base, IL-philic, and IL-phobic electrolytes (top), with their corresponding difference spectra (bottom). (c) Schematic diagram of water molecule distribution and H-bond formation at the anode/electrolyte interface. Reproduced with permission from Ref. [51]. Copyright©2025, the American Chemical Society.

morphology that prevents physical contact between the electrode and electrolyte; and (iv) sufficient mechanical robustness to withstand repeated cycling. SEI is insoluble product generated at the anode/electrolyte interface, decomposed of organic electrolytes, *i.e.*, solvent and salt. However, in traditional dilute aqueous electrolytes, the solvent (water) easily decomposes into gaseous products during Zn stripping/plating processes. This implies that salt, specifically the anion, is responsible for the formation of SEI. Therefore, one popular strategy is to increase the salt population in the electrolytes, trying to involve anions inside the primary solvation shell of Zn^{2+}. Additionally, another strategy is to include reactive species in aqueous electrolytes, such as functional anions ($TFSI^-$, OTF^-, and OAc^-), dissolved gases like CO_2, organic co-solvents (*e.g.*, trimethyl phosphate) and additives like urea [88–91].

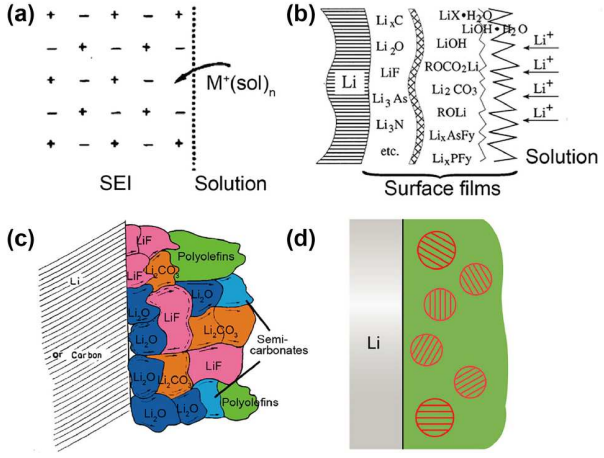

Figure 12 (Color online) Proposed models of SEI composition and their distribution. (a) The single crystal representation, (b) the multi-layered model, (c) the Mosaic model, and (d) the plum pudding model. Reproduced with permission from Ref. [87]. Copyright©2025, the Multidisciplinary Digital Publishing Institute.

It's worth noting that these SEI-forming precursors contain critical elements, such as nitrogen, fluorine and phosphorus as well as organic constituents, essential for forming traditional SEI components, including inorganic zinc salts and various organic species.

Therefore, ILs are excellent and promising precursors for *in-situ* forming a stable SEI in AZMBs, owing to their highly designable chemical structures and compositions. OTF-based ILs are usually employed in AZMBs because they are able to provide the critical elements, likewise in aqueous sodium-ion battery [92]. In 3 M $Zn(OTF)_2$ + 0.5 M [BMIM]OTF electrolyte, the X-ray photoelectron spectroscopy (XPS) results of the top surface of Zn anode revealed the adsorption of [BMIM] cations, C–N and C–S organic species, ZnS, ZnF_2, and $ZnSO_3$ inorganic components (Figure 13a). After sputtering for 5 min, the N 1s signal of C–N and the signal of inorganic zinc salt (*i.e.*, ZnF_2 and ZnS) became more pronounced, suggesting that the inorganic species are embedded in the organic components, which form a dense SEI. On the contrary, the signal of inorganic salts cannot be detected without the addition of [BMIM]OTF in the electrolyte even though $Zn(OTF)_2$ is also present in the electrolyte. The results demonstrate the excellent capability of [BMIM]OTF IL in promoting the formation of a stable and dense SEI in AZMBs. Undoubtedly, SEI formation is closely related to the increased formation of cation-anion CIPs in Zn^{2+} solvation structure, as discussed in the previous section. Differently, with the same concentration (3 M) of the $Zn(OTF)_2$-based electrolyte, the XPS results with a certain depth of Ar^+ sputtering revealed an inhomogeneous distribution of ZnF_2, ZnS, $ZnSO_3$, and $ZnCO_3$ (Figure 13b) in Chen's work [42]. In contrast, upon the introduction of [EMIM]FSI, a uniform SEI layer enriched in inorganic species (Figure 13c) was formed, resulting from the decomposition of Zn-anion complexes within the altered solvation structure. Building on the experimental investigations of SEI composition and distribution, they further studied the anion reduction chemistry through both experimental and theoretical approaches. This study is essential for understanding the chemistry

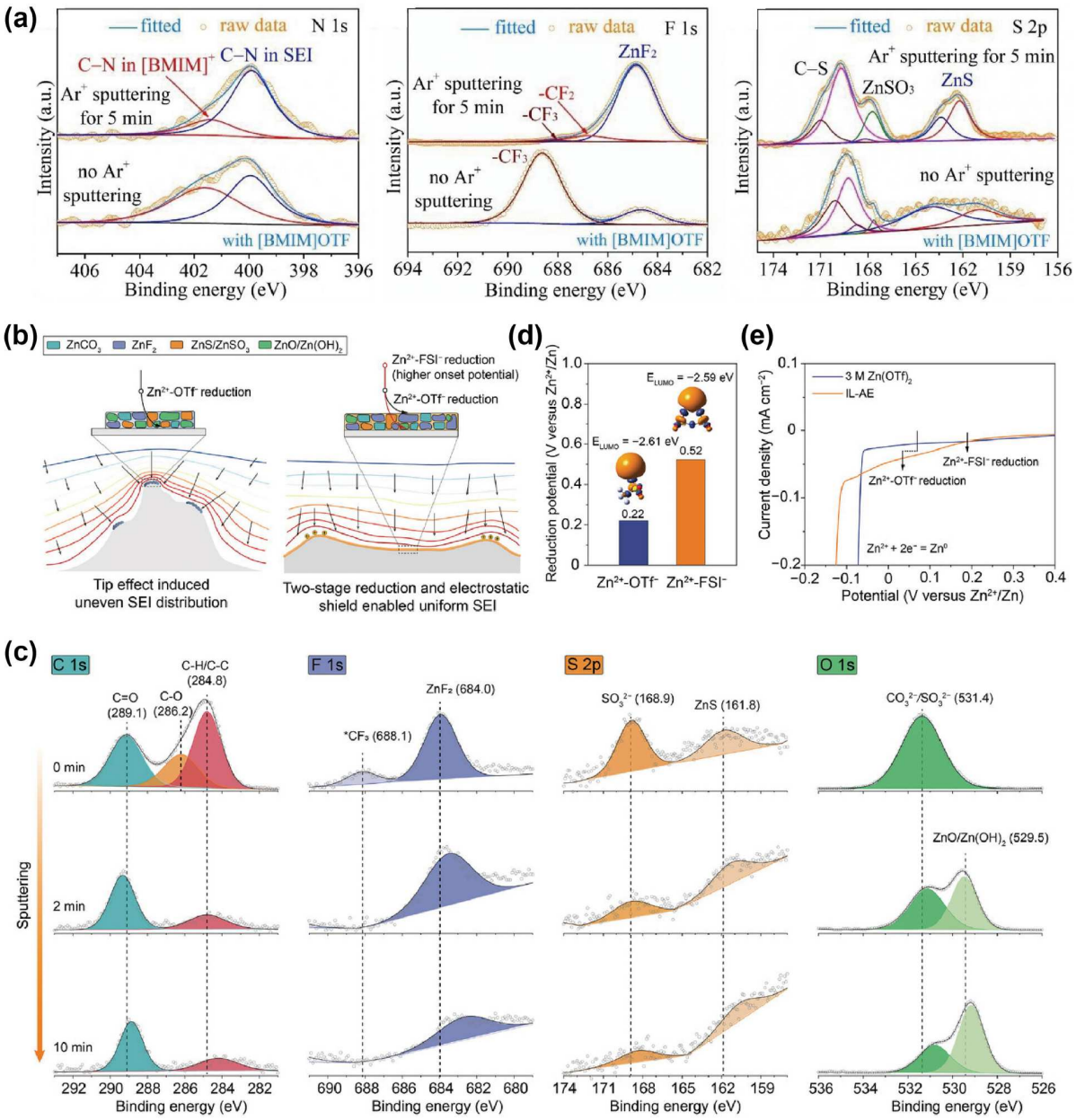

Figure 13 (Color online) (a) High resolution XPS spectra (N 1s, F 1s, and S 2p) without or with Ar^+ sputtering of Zn electrodes cycled in 3 M $Zn(OTF)_2$ + 0.5 M [BMIM]OTF electrolyte. Reproduced with permission from Ref. [57]. Copyright©2022, Elsevier. (b) Schematic diagram of the proposed SEI formation mechanisms and distribution in different electrolytes. (c) High-resolution XPS spectra (C 1s, F1s, S 2p, and O 1s) of cycled Zn electrodes in different electrolytes after Ar^+ sputtering for 0, 2, and 4 min. (d) The calculated anion reduction potential in Zn^{2+}-OTF^- and Zn^{2+}-FSI^- complexes. (e) Linear sweep voltammetry curves of 3 M $Zn(OTF)_2$ and IL-AE electrolytes. Reproduced with permission from Ref. [42]. Copyright©2023, Wiley-VCH.

behind SEI formation. Typically, the electrochemical reduction potential of OTF^- and FSI^- is out of the operating potential range of AZMBs. Nevertheless, when they are complexed with Zn-ions, the DFT simulation results suggest that the onset reduction potential (*vs.* Zn/Zn^{2+}) of Zn^{2+}-OTF^- and Zn^{2+}-FSI^- are 0.22 and 0.52 V, respectively (Figure 13d), which had been further proved by Linear sweep voltammetry curves (Figure 13e).

The *ex-situ* SEI derived from the IL typically presents itself in the form of a membrane, composed of polymeric IL, on the zinc surface. This protective layer is able to physically separate Zn anodes from continuous contact with aqueous electrolytes and confine Zn^{2+} flux by multiple ion channels, therefore suppressing parasitic reactions and guiding uniform Zn deposition. Earlier in 2021, the poly IL precursor consisted of $Zn(TFSI)_2$, 1-butyl-1-methylpyrrolidinium-TFSI and thiol-ene polymer compliant skeleton was spin-coated on the Zn surface, followed by irradiation-assisted curing [93]. The ideal thickness of this membrane was proved to be 500 nm, together with a smaller charge transfer resistance and longer cycling life in symmetrical Zn||Zn cell. This Zn-ion conductive membrane was confirmed to effectively suppress water-induced side reactions due to its hydrophobicity and enable uniform Zn^{2+} conduction through it at the same time. These advantages allow for stable cycling performance of a symmetrical Zn||Zn cell at an extremely high DOD of 90%. Later, Li's group [94] designed a poly IL layer based on CAVIm IL, employing the spin-coating method as well. Furthermore, they adjusted the ratio between IL monomer and crosslinker to delicately manipulate the morphology, realizing the best balance between ion permeability and selectivity. Besides, the coated poly IL layer effectively suppresses HER and side reactions. Notably, Chen *et al.* [95] proposed a multifunctional IL co-polymer protective layer

on top of the Zn surface. The two monomers are tert-butyl acrylate and [2-(methacryloyloxy)ethyl]dimethyl-(3-sulfopropyl). The former one possesses water-blocking functional groups, preventing water from penetrating through the polymer and then reaching the Zn surface. The latter one contains cations and anions, which are capable of modulating Zn^{2+} flux via strong interactions with Zn^{2+} and helping reduce charge transfer resistance. However, this membrane has a thickness of 10 μm, which is much thicker than 500 nm in the case of Lee's work [93].

4.3 Interfacial compatibility with cathodes (*e.g.*, Mn-based, V-based, conversion type)

The electrolyte composition not only has a profound impact on the Zn anode's performance but also exerts equally important effects on the cathode. Therefore, evaluating the compatibility between IL-based electrolytes and cathodes is essential to achieve the outstanding electrochemical performance required for practical zinc batteries.

Cathode materials based on manganese (*e.g.*, MnO_2) and vanadium (*e.g.*, $NH_4V_4O_{10}$, V_2O_5, NaV_3O_8) all suffer from a common and significant challenge which is the dissolution of their active materials [96]. For instance, the dissolution of the Mn element resulted from the transformation of MnO_2 when the cell voltage is lower than 1.56 V. Additionally, the intrinsic solubility of Mn^{2+} in water is relatively high, reaching 70 g in 100 mL H_2O at 7 °C. For V-based cathodes, vanadium dissolution primarily stems from pH fluctuations at the electrode/electrolyte interface and active-water attack. These pH fluctuations are triggered by two factors. One is the co-insertion of H^+ into the host cathode material and the other is the migration of OH^- from the anode, the latter being a product of the HER. Consequently, IL-modified electrolytes, which effectively suppress HER at the anode and lower the overall water activity, can mitigate vanadium dissolution and thereby enhance the electrochemical performance of V-based zinc full cells [59]. Additionally, the Zn||$Zn_{0.25}V_2O_5{\cdot}nH_2O$ full cell operating at a high temperature of 60 °C exhibited much better cycling performance compared to the electrolyte without IL (Figure 14a), demonstrating the superior electrochemical stability of IL at high temperatures. Conversely, the designed electrolyte demonstrates limited efficacy in improving the MnO_2 cathode performance, as the incorporation of IL fails to effectively mitigate the Mn^{2+} dissolution issue (Figure 14b).

The dissolution mechanism of halogen cathodes is more complex than those of the cathodes mentioned above. Taking the typical conversion-type iodine-based cathode as an example, the one-step

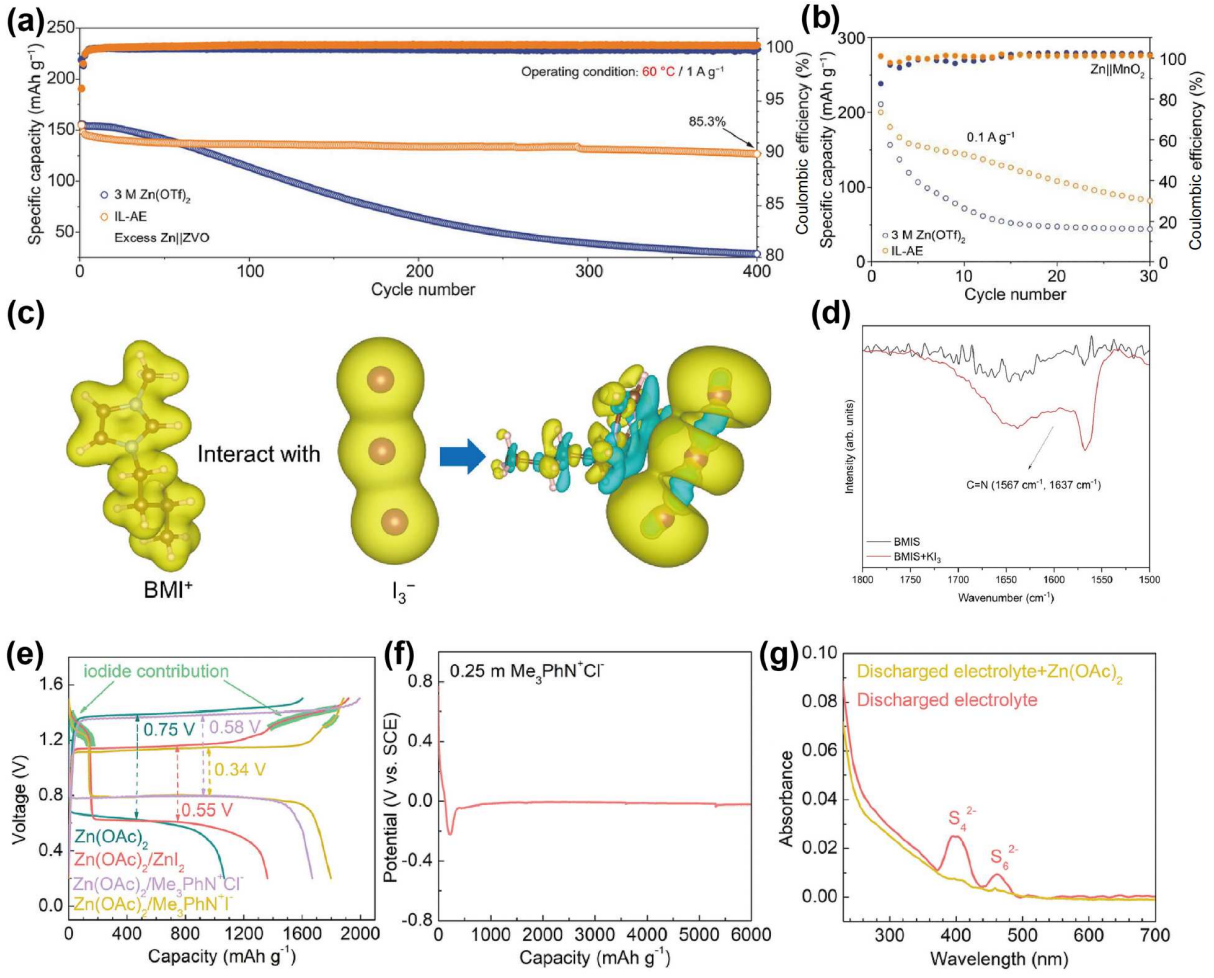

Figure 14 (Color online) (a) The long-term cycling stability of Zn||$Zn_{0.25}V_2O_5{\cdot}nH_2O$ full cells in different electrolytes under a current density 1 A g^{-1} of at 60 °C. (b) Cycling stability comparison of Zn||MnO_2 full cells in different electrolytes under a current density 1 A g^{-1}. Reproduced with permission from Ref. [42]. Copyright©2023, Wiley-VCH. (c) Charge density differences with I_3^- and $[BMIM]^+$. (d) ATR-FTIR spectra in the regions of 1500–1800 cm^{-1} of [BMIM]OTF aqueous solution and following addition of KI_3 solution. Reproduced with permission from Ref. [97]. Copyright©2024, the American Chemical Society. (e) Galvanostatic charge/discharge profiles of Zn-S cells in different electrolytes. (f) The discharge curve of S electrode in a 3-electrode cell with a saturated calomel electrode as reference electrode in 0.25 m $[Me_3PhN]^+Cl^-$ electrolyte at 0.1 A g^{-1}. (g) The UV-Vis spectra of the corresponding discharged electrolyte and following addition of zinc acetate in the regions of 230–700 nm^{-1}. Reproduced with permission from Ref. [100]. Copyright©20232, the Royal Society of Chemistry.

I^0/I^- redox reaction involves the intermittent formation of polyiodides (*e.g.*, I_3^- and I_5^-), which are highly soluble in aqueous solution. This liquid-liquid transition process enables rapid conversion kinetics. However, the resulting polyiodides can migrate toward the Zn anode on account of gradients, leading to the well-known shuttle effect of polyiodides. Imidazolium-based IL was found to be capable of forming N–I bonds (N of C–N in imidazole ring) with I_3^- and I_5^-, which is confirmed by both the simulation results and spectroscopy results (Figure 14c, d) [97]. This strategy molecularly suppresses the polyiodide shuttle issue, a mechanism not typically provided by traditional additives which often rely on electron affinity to I_3^- or I_5^- [98]. Therefore, the Zn||I_2 battery exhibited extraordinary electrochemical performance. Another promising conversion-type cathode material is sulfur due to its high theoretical capacity of 1675 mAh g^{-1}. In AZMBs, the S cathode goes through a solid-solid transition (S ⇋ ZnS), unlike in the multiple steps of S chemistry in non-aqueous lithium-ion batteries [99]. The solid-solid transition process, combined with the low electronic conductivity of S, lead to sluggish S reaction kinetics and comparatively high polarization of over 0.7 V at relatively low current densities. Quaternary ammonium iodide was proposed to facilitate the formation of soluble intermediates or reactants [100]. The reduction voltage of Zn||S cells was elevated from 0.6 to 0.8 V after introducing the 0.25 M IL to 1 M $ZnAc_2$ electrolyte (Figure 14e), confirming the enhanced S reduction chemistry. The soluble intermediates of polysulfides were also revealed by experimental and simulation results (Figure 14f, g).

5 Summary and outlook

The zinc metal anode is a promising solution to achieve high-energy-density aqueous batteries [14]. ILs, with their tunable structures, excellent electrochemical stability and low flammability, have been employed to enhance the electrochemical performance of zinc anodes in AZMBs. In this review, we systematically examine recent advances in the use of ILs in AZMBs, categorizing them based on their modes of incorporation into aqueous electrolytes. Special emphasis is placed on the interactions between ILs and water or zinc ions, particularly regarding solvation structures and hydrogen bond formation. We further explore the interfacial chemistry, including the formation of the SEI and the structure of the EDL, both of which are highly influenced by their specific chemical structures and compositions. A unified schematic illustrating the multi-scale protective roles of ILs for stable zinc anodes is summarized in Figure 15, complementing the existing Figure 1. Based on the above discussion, it can be concluded that the structural diversity and tunability of ILs contribute to suppressed water activity both in the bulk electrolyte and at the anode/electrolyte interface, as well as to modifications in the solvation structure and the formation of a protective SEI layer. These advantages of IL largely boost the electrochemical performance of zinc anodes in terms of suppressed side reactions, prolonged lifespan and excellent reversibility. However, despite great progress, challenges still remain in the application of ILs for AZMBs as demonstrated in the following aspects.

(1) The high cost and complex synthesis processes of ILs remain major obstacles to their practical application in AZMBs, as is the case in many other fields. Using ILs directly as supporting salts significantly raises the cost of hybrid aqueous electrolytes. The multi-step synthesis involved in producing ILs is a primary reason for their high expense. Therefore, developing task-specific ILs tailored for AZMBs, leveraging versatile cationic and anionic synergies (such as concurrently buffering the local pH and promoting the formation of a stable SEI), to achieve multifunction with a smaller dosage, as well as bio-derived and easily scalable ILs, represents a promising direction for reducing costs. Besides, machine learning can be employed to predict the relationship between the structure of IL and properties, providing guidance for researchers to find the most promising IL-based electrolytes.

(2) More future breakthroughs in AZMB electrolytes can stem from the synergistic combination of ILs with other advanced strategies. ILs integrated with high-concentration electrolytes are expected to further suppress water activity and expand the electrochemical window. Additionally, blending ILs with co-solvents enables precise tuning of solvation structure and physicochemical properties, such as HER-free and anti-freezing capability. Moving beyond single-component optimization, these hybrid systems represent a promising pathway towards designing high-performance and durable electrolytes for practical AZMBs.

(3) The working mechanisms of ILs in AZMBs remain incompletely understood. Even though intensive spectroscopy studies (FTIR, Raman and nuclear magnetic resonance spectroscopy) have been

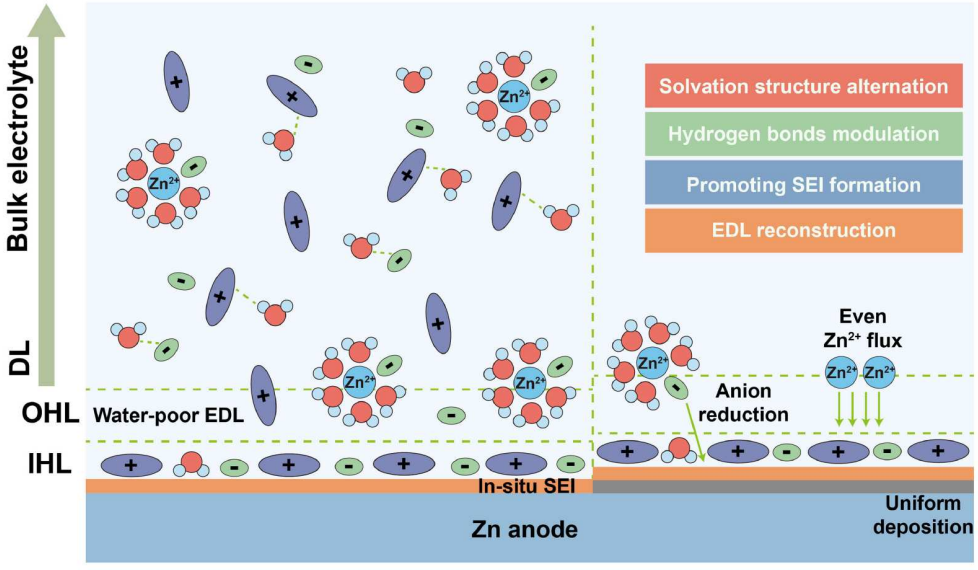

Figure 15 (Color online) A unified schematic illustration demonstrating the multi-scale protective roles of ILs for stable zinc anodes.

carried out to reveal the water activity, most cases of the solvation structure of Zn^{2+} in different electrolytes were studied by theoretical simulations. Additionally, the existence of conflicting interpretations in literature underscores the necessity for employing more sophisticated techniques to reveal the true mechanisms. In this regard, the application of *in-situ* and other high-precision methods to study the electrode/electrolyte interface will be paramount for gaining a deeper understanding of these dynamic processes.

(4) Most cathode materials with low mass loading are initially tested in coin cells using a zinc-rich anode. However, factors such as low areal capacity of the cathode, low zinc utilization, and excess electrolyte decrease the practical energy density of the cells. Therefore, the reliability of IL-based electrolytes for AZMBs must be reassessed under more rigorous conditions.

We do hope this review will inspire more research on the application of ILs in AZMBs, including task-specific and cost-effective IL design, integrating ILs with other approaches, deep understanding of working mechanisms and battery-level cell assembly under lean-electrolyte conditions for achieving real high-energy-level ZMBs.

Conflict of interest

The authors declare no conflict of interest.

Acknowledgement

This work was supported by the Australian Research Council (DE230100471), the Marie Skłodowska-Curie Actions (MSCA) (101152353) and the Natural Science Foundation of Jiangsu Province (BK20250590).

Funding note

Open Access funding enabled and organized by CAUL and its Member Institutions.

References

1 Yamamoto T, Shoji T. *Inorg Chim Acta*, 1986, 117: L27–L28
2 Hao J, Li X, Zeng X, Li D, Mao J, Guo Z. *Energy Environ Sci*, 2020, 13: 3917–3949
3 Chao D, Zhou W, Xie F, Ye C, Li H, Jaroniec M, Qiao SZ. *Sci Adv*, 2020, 6: eaba4098
4 Ju Z, Zheng T, Zhang B, Yu G. *Chem Soc Rev*, 2024, 53: 8980–9028
5 Demir-Cakan R, Palacin MR, Croguennec L. *J Mater Chem A*, 2019, 7: 20519–20539
6 Wan F, Zhou X, Lu Y, Niu Z, Chen J. *ACS Energy Lett*, 2020, 5: 3569–3590
7 Xu J, Li H, Jin Y, Zhou D, Sun B, Armand M, Wang G. *Adv Mater*, 2024, 36: 2309726
8 Shin J, Lee J, Park Y, Choi JW. *Chem Sci*, 2020, 11: 2028–2044
9 Liang Y, Yao Y. *Nat Rev Mater*, 2023, 8: 109–122
10 Wang Q, Zhou W, Zhang Y, Jin H, Li X, Zhang T, Wang B, Zhao R, Zhang J, Li W, Qiao Y, Jia C, Zhao D, Chao D. *Natl Sci Rev*, 2024, 11: nwae230
11 Chacko B, Madhuri W. *Battery Energy*, 2026, 5: e70066
12 Han C, Li W, Liu HK, Dou S, Wang J. *Nano Energy*, 2020, 74: 104880
13 Li Y, Wang H, Wu T, Xie C, Yang Z, Zhang Q, Sun D, Tang Y, Fu L, Wang H. *Sci China Chem*, 2023, 66: 1844–1853
14 Tan Y, Pu J, Li H, Chao D. *Sci China Chem*, 2024, 67: 4085–4097
15 Li X, Wang X, Ma L, Huang W. *Adv Energy Mater*, 2022, 12: 2202068
16 Rana A, Roy K, Heil JN, Nguyen JH, Renault C, Tackett BM, Dick JE. *Adv Energy Mater*, 2024, 14: 2402521
17 Cao Z, Zhuang P, Zhang X, Ye M, Shen J, Ajayan PM. *Adv Energy Mater*, 2020, 10: 2001599
18 Zeng Y, Luan D, Lou XWD. *Chem*, 2023, 9: 1118–1146
19 Cao L, Bu F, Wang Y, Gao Y, Zhao W, Yang J, Chen J, Xu X, Guan C. *Sci China Mater*, 2025, 68: 897–905
20 Gu W, Wu K, Huang J, Yang X, Huang X, Dong Z, Shen S, Bai Y, Liu H, Dou S, Wu C. *Adv Energy Mater*, 2025, 15: 2502652
21 Lv Y, Xiao Y, Ma L, Zhi C, Chen S. *Adv Mater*, 2022, 34: 2106409
22 Dong Q, Nian Q, Luo X, Fan J, Jiang J, Cui Z, Ruan D, Ren X. *Sci China Chem*, 2025, 68: 526–535
23 Li Z, Xie M, Wu Y, Fu K, Wang L, Zhang J, Chen S, Huang L, Liu C, Ma D, Huang H, Liao Y, Zeng F, Liang X. *Sci China Mater*, 2025, 68: 4516–4525
24 Yan H, Li S, Zhong J, Li B. *Nano-Micro Lett*, 2023, 16: 15
25 Yin Z, Yan X, Liu Y, Gao Z, Li Z, Qin Z, Zhang J, Wu Z, Hu W. *Sci China Mater*, 2025, 68: 3288–3294
26 Jiang X, Xiao K, Hu T, Yuan K, Chen Y. *Sci China Mater*, 2025, 68: 1946–1958
27 Su C, Gao X, Liu K, He A, He H, Zhu J, Liu Y, Chen Z, Zhao Y, Zong W, Dai Y, Lin J, Dong H. *Green Energy Intell Transp*, 2023, 2: 100126
28 Lin F, Wang C, Zou W, Ren Z, Gu K, Gao T, Tang Y, Zhang Y. *Sci China Mater*, 2026, 69: https://doi.org/10.1007/s40843-025-3449-5
29 Zhou W, Zhang M, Kong X, Huang W, Zhang Q. *Adv Sci*, 2021, 8: 2004490
30 Yan Q, Liu Y, Zhu W, Xu S, Law HM, Li J, Ciucci F. *Adv Funct Mater*, 2025, 36: e12706
31 Chen K, Xu Y, Li H, Li Y, Zhang L, Guo Y, Xu Q, Li Y, Xie H. *Chem Sci*, 2025, 16: 8648–8660
32 Su K, Bian Z, Mu Y, Lu Z, Wang Y, Li M, Zhao J, Lang J, Xu B. *Energy Storage Mater*, 2025, 81: 104480
33 Guo HJ, Chen XJ, Shu R, Zhong XB, Zhang LX, Song YX. *J Colloid Interface Sci*, 2025, 678: 627–636
34 Marsh KN, Boxall JA, Lichtenthaler R. *Fluid Phase Equilib*, 2004, 219: 93–98
35 Walden P. *Bull Acad Imper Sci (St Petersburg)*, 1914, 1800: 405–422
36 Wilkes JS, Zaworotko MJ. *J Chem Soc Chem Commun*, 1992, 13: 965–967
37 Fuller J, Carlin RT, Osteryoung RA. *J Electrochem Soc*, 1997, 144: 3881–3886
38 Choudhury AR, Winterton N, Steiner A, Cooper AI, Johnson KA. *CrystEngComm*, 2006, 8: 742–745
39 Araújo JMM, Pereiro AB, Alves F, Marrucho IM, Rebelo LPN. *J Chem ThermoDyn*, 2013, 57: 1–8
40 Han J, Mariani A, Passerini S, Varzi A. *Energy Environ Sci*, 2023, 16: 1480–1501
41 Zhou T, Chen L, Ye Y, Chen L, Qi Z, Freund H, Sundmacher K. *Ind Eng Chem Res*, 2012, 51: 6256–6264
42 Yu L, Huang J, Wang S, Qi L, Wang S, Chen C. *Adv Mater*, 2023, 35: 2210789
43 Paduszyński K. *Ind Eng Chem Res*, 2019, 58: 17049–17066
44 Pereira J, Souza R, Moita A. *Inorganics*, 2024, 12: 186
45 Ghandi K. *Green Sustain Chem*, 2014, 04: 44–53
46 Lewandowski A, Świderska-Mocek A. *J Power Sour*, 2009, 194: 601–609
47 Greaves TL, Drummond CJ. *Chem Rev*, 2008, 108: 206–237
48 Ue M, Murakami A, Nakamura S. *J Electrochem Soc*, 2002, 149: A1572
49 Yang F, Yuwono JA, Hao J, Long J, Yuan L, Wang Y, Liu S, Fan Y, Zhao S, Davey K, Guo Z. *Adv Mater*, 2022, 34: 2206754
50 Fei H, Yang F, Yuwono JA, Zarrabeitia M, Passerini S, Varzi A. *Chem Eng J*, 2024, 502: 157842
51 Zhao Q, Yu X, Wang J, Xue J, Ru Y, Zou Y, Qiao Y, Sun SG. *Nano Lett*, 2025, 25: 7385–7392
52 Agmon N. *Chem Phys Lett*, 1995, 244: 456–462
53 Li Q, Jiang J, Li G, Zhao W, Zhao X, Mu T. *Sci China Chem*, 2016, 59: 571–577
54 Abbott AP, Barron JC, Frisch G, Gurman S, Ryder KS, Fernando Silva A. *Phys Chem Chem Phys*, 2011, 13: 10224–10231
55 Ma L, Chen S, Li N, Liu Z, Tang Z, Zapien JA, Chen S, Fan J, Zhi C. *Adv Mater*, 2020, 32: e1908121
56 Xu H, Yang W, Li M, Liu H, Gong S, Zhao F, Li C, Qi J, Wang H, Peng W, Liu J. *Small*, 2024, 20: 2310972
57 Chen J, Zhou W, Quan Y, Liu B, Yang M, Chen M, Han X, Xu X, Zhang P, Shi S. *Energy Storage Mater*, 2022, 53: 629–637
58 Zhong M, Wang Y, Xie Y, Yuan S, Ding K, Begin EJ, Zhang Y, Bao JL, Wang Y. *Adv Funct Mater*, 2024, 34: 2316788
59 Xiao T, Yang J, Zhang B, Wu J, Li J, Mai W, Fan HJ. *Angew Chem Int Ed*, 2024, 63: e202318470
60 Gomez Vazquez D, Pollard TP, Mars J, Yoo JM, Steinrück HG, Bone SE, Safonova OV, Toney MF, Borodin O, Lukatskaya MR. *Energy Environ Sci*, 2023, 16: 1982–1991
61 Shen C, Zhang Y, Li X, Guo P, Zeng X, Ni K, Cao R, Wang Z, Wang Z, Qin L. *J Mater Chem A*, 2025, 13: 2174–2186
62 Zhao Z, Lai J, Ho DT, Lei Y, Yin J, Chen L, Schwingenschlögl U, Alshareef HN. *ACS Energy Lett*, 2022, 8: 608–618
63 Su K, Zhang H, Wang Y, Zhang X, Mu Y, Lu Z, Han Y, Wan S, Lang J. *Chem Eng J*, 2024, 496: 153927
64 Li S, Xu M, Chen K, Wu Q, Li Y, Xie C, Li Y, Xu Q, Huang J, Xie H. *J Colloid Interface Sci*, 2025, 678: 934–947
65 Qiu M, Xin Y, Liang Y, Liu Y, Chen J, Li J, Sun P, Fan HJ, Mai W. *Adv Mater*, 2025, 37: 2418947
66 Solanki S, Jha S, Sappidi P, Gupta PK. *J Power Sour*, 2025, 656: 238019
67 Song YX, Wang J, Zhong XB, Zhang YH, Wang K, Guo XH, Guo HJ, Lei GP, Liu HT, Wang GK, Ji PG, Zhang X, Khalilov U, Liang JF, Wen R. *J Colloid Interface Sci*, 2024, 665: 711–719
68 Liu C, Xu W, Zhang L, Zhang D, Xu W, Liao X, Chen W, Cao Y, Li M, Mei C, Zhao K. *Angew Chem Int Ed*, 2024, 63: e202318063
69 Weng J, Zhu W, Yu K, Luo J, Chen M, Li L, Zhuang Y, Xia K, Lu Z, Hu Y, Yang C,

Wu M, Zou Z. *Adv Funct Mater*, 2024, 34: 2314347
70 Behera A, Deb D, Bhattacharyya AJ. *J Mater Chem A*, 2025, 13: 33784–33797
71 Lv Y, Huang C, Zhao M, Fang M, Dong Q, Tang W, Yang J, Zhu X, Qiao X, Zheng H, Sun C, Zheng L, Zheng M, Xu Y, Lu J. *J Am Chem Soc*, 2025, 147: 8523–8533
72 Handy S. *Curr Org Chem*, 2005, 9: 959–988
73 Cao L, Li D, Pollard T, Deng T, Zhang B, Yang C, Chen L, Vatamanu J, Hu E, Hourwitz MJ, Ma L, Ding M, Li Q, Hou S, Gaskell K, Fourkas JT, Yang XQ, Xu K, Borodin O, Wang C. *Nat Nanotechnol*, 2021, 16: 902–910
74 Qi W, Zhang W, Niu Z, Niu L, Zhang H, Jiang F, Zhou X, Kumar A, Li L, Wang J, Sun J. *Sci China Chem*, 2025, 68: 2088–2095
75 Li M, Wang X, Meng J, Zuo C, Wu B, Li C, Sun W, Mai L. *Adv Mater*, 2023, 36: 2308628
76 Zhang J, Song XM, Sun Z, Liu D, Song Z, Li S. *J Energy Storage*, 2025, 125: 116985
77 Li T, Liu J, Shu H, Sun A, Zhao T, Chen Y, Chen Y. *Adv Funct Mater*, 2026, 36: e14358
78 Zhang T, Shi X, Li Y, Sangaraju S, Wang F, Yang L, Ran F. *Mater Rep-Energy*, 2024, 4: 100272
79 Chen Y, Zhu M, Li C, Wang H, Chen D, Wu H, Huang Z, Wang Y, Fan Y, Bai Z, Chen S, Tang Y, Zhang Y. *Adv Funct Mater*, 2025, 35: 2501162
80 Hu Z, Han Z, Liu H, Jiang X, Bai K, Huang S, Yang Z, Ye M, Tang Y, Zhang Y, Liu X, Wen Z, Park HS, Li CC. *J Am Chem Soc*, 2025, 147: 46632–46641
81 Xu M, Liu F, Chen L, Lei Y, Liu Z, Abdiryim T, Xu F, You J, Tan Y, Tan Z, Liu X. *Energy Storage Mater*, 2025, 80: 104373
82 Xu Y, Chen K, Xu M, Li Y, Wu Q, Li S, Xie C, Li Y, Xie H, Huang J. *Energy Environ Sci*, 2025, 18: 1560–1571
83 Yan C, Yuan H, Park HS, Huang JQ. *J Energy Chem*, 2020, 47: 217–220
84 Yan C, Xu R, Xiao Y, Ding J, Xu L, Li B, Huang J. *Adv Funct Mater*, 2020, 30: 1909887
85 Jiang L, Li D, Xie X, Ji D, Li L, Li L, He Z, Lu B, Liang S, Zhou J. *Energy Storage Mater*, 2023, 62: 102932
86 Peled E. *J Electrochem Soc*, 1979, 126: 2047–2051
87 Wei Z, Zheng W, Li Y, Huang S. *Nanomaterials*, 2025, 15: 554
88 Suo L, Borodin O, Gao T, Olguin M, Ho J, Fan X, Luo C, Wang C, Xu K. *Science*, 2015, 350: 938–943
89 Zhou Y, Shen H, Chen X, Liu C, Shan X, Wang W, Chen Z. *J Electrochem Soc*, 2024, 171: 040513
90 Yue J, Zhang J, Tong Y, Chen M, Liu L, Jiang L, Lv T, Hu Y, Li H, Huang X, Gu L, Feng G, Xu K, Suo L, Chen L. *Nat Chem*, 2021, 13: 1061–1069
91 Li Q, Yang C, Zhang J, Ji X, Xu J, He X, Chen L, Hou S, Uddin J, Addison D, Sun D, Wang C, Wang F. *Angew Chem Int Ed*, 2022, 61: e202214126
92 Suo L, Borodin O, Wang Y, Rong X, Sun W, Fan X, Xu S, Schroeder MA, Cresce AV, Wang F, Yang C, Hu Y, Xu K, Wang C. *Adv Energy Mater*, 2017, 7: 1701189
93 Lee D, Kim H, Kim W, Cho S, Baek K, Jeong K, Ahn DB, Park S, Kang SJ, Lee S. *Adv Funct Mater*, 2021, 31: 2103850
94 Zheng S, Wei L, Zhang Z, Pan J, He J, Gao L, Li CC. *Nano Lett*, 2022, 22: 9062–9070
95 Lv Y, Xiao Y, Xu S, Huo F, Chen Y, Zhao M, Liu L, Su C, Zhu Y, Chen S. *J Mater Chem A*, 2022, 10: 16952–16961
96 Li G, Sun L, Zhang S, Zhang C, Jin H, Davey K, Liang G, Liu S, Mao J, Guo Z. *Adv Funct Mater*, 2024, 34: 2301291
97 Wu H, Hao J, Zhang S, Jiang Y, Zhu Y, Liu J, Davey K, Qiao SZ. *J Am Chem Soc*, 2024, 146: 16601–16608
98 Shen T, Li X, Wang H, Zhou A, Liu M, Xu M, Tao B, Tian W, Zhao Y. *Small*, 2025, 21: 2507166
99 Li BQ, Zhang Q. *Sci China Chem*, 2021, 64: 337–338
100 Wu W, Wang S, Lin L, Shi HY, Sun X. *Energy Environ Sci*, 2023, 16: 4326–4333